9650 *Biochemistry* **2009,** *48,* 9650–9667
DOI: 10.1021/bi900887k

BIOCHEMISTRY
including biophysical chemistry & molecular biology
Article

Crystal Structure and Catalytic Properties of *Bacillus anthracis* CoADR-RHD: Implications for Flavin-Linked Sulfur Trafficking[†,‡]

Jamie R. Wallen,[§,∥] T. Conn Mallett,[§,⊥] William Boles,[§] Derek Parsonage,[§] Cristina M. Furdui,[#] P. Andrew Karplus,[Δ] and Al Claiborne*[,§]

[§]*Center for Structural Biology and* [#]*Section on Molecular Medicine, Department of Internal Medicine, Wake Forest University School of Medicine, Winston-Salem, North Carolina 27157, and* [Δ]*Department of Biochemistry and Biophysics, Oregon State University, Corvallis, Oregon 97331.* [∥]*Present address: Department of Biochemistry and Molecular Biophysics, Washington University School of Medicine, St. Louis, MO 63110.* [⊥]*Present address: Rigaku, Sevenoaks, Kent TN15 6QY, England.*

Received May 26, 2009; Revised Manuscript Received August 13, 2009

ABSTRACT: Rhodanese homology domains (RHDs) play important roles in sulfur trafficking mechanisms essential to the biosynthesis of sulfur-containing cofactors and nucleosides. We have now determined the crystal structure at 2.10 Å resolution for the *Bacillus anthracis* coenzyme A-disulfide reductase isoform (*Ba*CoADR-RHD) containing a C-terminal RHD domain; this is the first structural representative of the multidomain proteins class of the rhodanese superfamily. The catalytic Cys44 of the CoADR module is separated by 25 Å from the active-site Cys514′ of the RHD domain from the complementary subunit. In stark contrast to the *B. anthracis* CoADR [Wallen, J. R., Paige, C., Mallett, T. C., Karplus, P. A., and Claiborne, A. (2008) *Biochemistry 47*, 5182−5193], the *Ba*CoADR-RHD isoform does not catalyze the reduction of coenzyme A-disulfide, although both enzymes conserve the Cys-SSCoA redox center. NADH titrations have been combined with a synchrotron reduction protocol for examination of the structural and redox behavior of the Cys44-SSCoA center. The synchrotron-reduced (Cys44 + CoASH) structure reveals ordered binding for the adenosine 3′-phosphate 5′-pyrophosphate moiety of CoASH, but the absence of density for the pantetheine arm indicates that it is flexible within the reduced active site. Steady-state kinetic analyses with the alternate disulfide substrates methyl methanethiolsulfonate (MMTS) and 5,5′-dithiobis(2-nitrobenzoate) (DTNB), including the appropriate Cys → Ser mutants, demonstrate that MMTS reduction occurs within the CoADR active site. NADH-dependent DTNB reduction, on the other hand, requires communication between Cys44 and Cys514′, and we propose that reduction of the Cys44-SSCoA disulfide promotes the transfer of reducing equivalents to the RHD, with the swinging pantetheine arm serving as a ca. 20 Å bridge.

As reviewed by Mueller (*1*), nature seems to have settled on protein persulfide groups (R-SSH) rather than toxic bisulfide (HS^-) as the dominant source of S^{2-} equivalents for biosynthesis of sulfur-containing cofactors and thionucleosides. In the latter category, the biosynthesis of 4-thiouridine at position 8 in tRNA is catalyzed in *Escherichia coli* by ThiI (*2*, *3*), a rhodanese homology domain (RHD)[1] protein that forms a persulfide derivative of Cys456 (Cys456-SSH) within the RHD domain. Transfer of the terminal sulfur to the O4-adenylated U8-tRNA intermediate is proposed to yield an intramolecular protein disulfide between Cys456 and Cys344 of the ThiI PP-loop domain. A similar sulfur transfer mechanism has been considered for the human molybdopterin synthase sulfurase MOCS3 (*4*−*6*); to the best of our knowledge, however, no crystal structures have been reported for either of these RHD proteins. The role of the *E. coli* ThiI RHD protein in 4-thiouridine synthesis has been contrasted with the biosynthesis of 2-thiouridine at position 34 in specific (Lys, Gln, and Glu) tRNAs (*7*); in the latter case, the five *E. coli* Tus proteins (TusA−E) provide a Cys-SSH-based sulfur relay system that traffics a sulfur atom from free Cys, through a cascade of protein persulfide intermediates hosted on TusA, TusD, and TusE, to the 2-thiouridine product. Structures have been reported for TusA (*8*), for the TusBCD complex (*9*), and for the terminal MnmA thiouridylase−tRNA complex (*10*). The recent structural and functional analysis of the sulfur oxidation ($S^0 \rightarrow SO_4^{2-}$) pathway in the purple sulfur bacterium *Allochromatium vinosum* (*11*) has identified key similarities

[†]This work was supported by National Institutes of Health Grant GM-35394 (A.C.), by WFUSM Development Funds (C.M.F.), and by National Science Foundation Grant MCB-9982727 (P.A.K.). Data for this study were measured at beamlines X12C and X26C of the National Synchrotron Light Source. Financial support comes principally from the Offices of Biological and Environmental Research and of Basic Energy Sciences of the U.S. Department of Energy and from the National Center for Research Resources of the National Institutes of Health.

[‡]Coordinates have been deposited with the Protein Data Bank as entries 3ICR, 3ICS, and 3ICT.

*To whom correspondence should be addressed. Telephone: (336) 716-3914. Fax: (336) 777-3242. E-mail: alc@csb.wfu.edu.

[1]Abbreviations: RHD, rhodanese homology domain; CoADR, coenzyme A-disulfide reductase; CoADR-RHD, coenzyme A-disulfide reductase isoform with a C-terminal rhodanese homology domain; DTNB, 5,5′-dithiobis(2-nitrobenzoate); CoAD, coenzyme A-disulfide; MMTS, methyl methanethiolsulfonate; *Sa*CoADR, *Staphylococcus aureus* coenzyme A-disulfide reductase; *Ba*CoADR-RHD, *Bacillus anthracis* coenzyme A-disulfide reductase isoform with a C-terminal rhodanese homology domain; *Ba*CoADR, *B. anthracis* coenzyme A-disulfide reductase; SeMet, selenomethionine; TNB, 2-nitro-5-thiosulfobenzoate; MAD, multiwavelength anomalous dispersion; LAB, data set collected in-house using a rotating anode X-ray source; SYNC1, synchrotron data set (*peak1*) collected over the first 180°; SYNC6, final synchrotron data set (*inflection2*); ESI-TOF, electrospray ionization time-of-flight; GR, glutathione reductase; CoAS-II, assigned half of coenzyme A-disulfide corresponding to the first CoASH product during reduction; EH_2, two-electron reduced enzyme; EH_4, four-electron reduced enzyme; E, oxidized enzyme; PDB, Protein Data Bank.

 Published on Web 09/02/2009

Scheme 1: Proposed Mechanism for Polysulfide Formation by Sulfide:Quinone Oxidoreductase

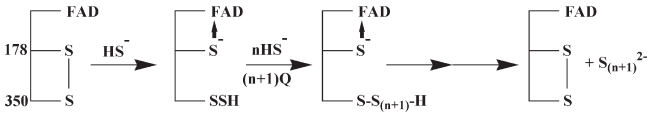

Scheme 2: One Proposed Role for the RHD Domain in *Sh. loihica* CoADR-RHD

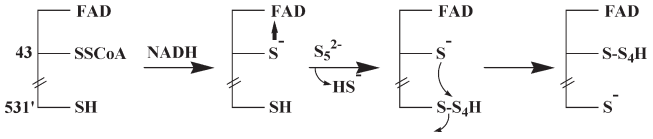

between the *E. coli* Tus system and the Dsr proteins that comprise a sulfur trafficking portal for delivery of persulfidic S^0 from the periplasm to the cytoplasmic sulfur oxidation machinery.

Very recently, the participation of "flavoprotein disulfide reductases" has been demonstrated in sulfur trafficking and/or sulfide metabolism in prokaryotes. Brito et al. (*12*) have determined the crystal structure of an archaeal sulfide:quinone oxidoreductase; in addition to the active-site Cys178 and Cys350, located proximal to the covalently bound FAD isoalloxazine on the *re* face, a chain of three sulfur atoms is identified bridging the two Cys residues. These and other observations, including the active-site Cys161−Cys337 disulfide identified in the closely related structure of the *A. vinosum* flavocytochrome *c* sulfide dehydrogenase (*13*; flavoprotein subunit), have led to a mechanistic proposal (Scheme 1) in which repeated cycles of (1) HS^- attack on Cys350 of the disulfide and (2) electron transfer from the nascent Cys178-S^-, via the flavin, to quinone allow extension of the polysulfide chain attached to Cys350. In a final step for which the chemical details are less clear, the Cys178−Cys350 disulfide is re-formed and the polysulfide product is released. Although sulfide:quinone oxidoreductase and flavocytochrome *c* sulfide dehydrogenase are members of the NADH dehydrogenase subgroup of the "two-dinucleotide binding domains" flavoproteins superfamily (*14*) that also includes the flavoprotein disulfide reductases (*15*), the second dinucleotide binding domain in these two enzymes does not bind NAD(P)H; HS^- replaces the pyridine nucleotide as the hydride donor. Furthermore, Cys178 and Cys350 do not correspond to any of the active-site Cys motifs identified in the flavoprotein disulfide reductases.

In our report on the crystal structure of coenzyme A-disulfide reductase (CoADR) from *Staphylococcus aureus* (*16*), we identified novel bacterial CoADR isoforms containing C-terminal extensions, including an RHD. The CoADR-RHD proteins link the CoADR module (ca. 450 residues) with a C-terminal RHD domain (ca. 110 residues); thus far, the one CoADR-RHD protein characterized is that from the sulfur-reducing facultative anaerobe *Shewanella loihica* PV-4 (*17*). The recombinant *Sh. loihica* protein catalyzed the NADH-dependent reductions of both polysulfide [S_n^{2-}, where n = 4 and 5 species are predominant at the assay pH of 8.0 (*18*); k_{cat} = 28 s^{-1}] and DTNB [k_{cat}/K_m(DTNB) = 1.7 × 10^5 M^{-1} s^{-1}]. Although CoADR is a functional flavoprotein disulfide reductase [group 3 (*15*)], CoADR-RHD did not catalyze the reduction of CoAS-disulfide (CoAD) as do the *S. aureus* (*19*) and *Bacillus anthracis* (*20*) CoADRs. The purified *Sh. loihica* enzyme gave a visible absorption spectrum characteristic of a flavoprotein, but anaerobic addition of 5 equiv of NADH/FAD reduced only ca. 50% of the flavin. Lukose et al. (*17*) suggested two possible roles for the RHD domain in S_n^{2-} reduction (Scheme 2), in either (1) delivery of bound S_n^{2-} to the active-site Cys43 of the CoADR module or (2) thiol−polysulfide interchange with a Cys43-SS_nH intermediate, yielding a Cys43-SSH persulfide for reduction. While either scheme could in principle lead to full reduction of S_n^{2-} to $n$$HS^-$, neither restores the Cys43-SSCoA disulfide presumed to exist in the oxidized enzyme.

We have selected *B. anthracis* as a model organism for investigations into unique CoASH biosynthetic and redox functions, as in this organism CoASH replaces GSH as the major low-molecular weight thiol (*21*). While *Bacillus subtilis* also lacks GSH, Cys has been shown to be the major low-molecular weight thiol in one report (*22*), and the four *B. subtilis* strains represented in the National Center for Biotechnology Information database lack both CoADR and CoADR-RHD isoforms.[2] Given the increased level of expression of the BAS0736 gene encoding CoADR-RHD in *B. anthracis* Sterne late in sporulation (*23*), the absence of structural representatives for multidomain enzymes containing the RHD (*1*, *24*), and the well-defined structures and mechanisms for the CoADR enzymes from *B. anthracis* (*20*) and *S. aureus* (*16*, *19*) [another GSH-deficient organism (*22*)], we have undertaken kinetic and spectroscopic studies of the *B. anthracis* CoADR-RHD, based on the alternate disulfide substrates MMTS and DTNB. We also present the crystal structures for both oxidized (FAD, Cys44-SSCoA) and synchrotron-reduced (FAD, Cys44-SH + CoASH) forms of CoADR-RHD, along with a mass spectrometric analysis of enzyme inactivation during NADH:MMTS oxidoreductase turnover.

EXPERIMENTAL PROCEDURES

Expression and Purification of Wild-Type and Mutant SaCoADRs and CoADR-RHDs. Expression and purification of *Sa*CoADR followed the published protocol (*19*). The *Ba*CoADR-RHD clone (Ames strain; BA0774) was provided by T. Blank and A. Friedlander (U.S. Army Medical Research Institute of Infectious Diseases, Fort Detrick, MD). The protein was expressed with an N-terminal His tag provided by the pTHCm (*25*) plasmid vector in *E. coli* B834(DE3) cells. The expression and purification protocol followed that described recently for *Ba*CoADR (*20*), with the following exceptions: expression cultures contained 50 μg/mL chloramphenicol and were harvested 8−9 h after induction; there were small differences in resuspension and Q-Sepharose loading buffers; and the Ni Sepharose High Performance (GE Healthcare) protocol described for *Ba*CoADR Tyr → Phe mutants was employed. The purified CoADR-RHD protein was buffer-exchanged into 50 mM potassium phosphate (pH 7.0) containing 0.5 mM EDTA, concentrated to 10 mg/mL prior to addition of glycerol to a final concentration of 20% (v/v), flash-frozen in liquid nitrogen, and stored in 0.05−0.5 mL aliquots at −80 °C. The expression and purification of SeMet CoADR-RHD were essentially identical to that described for the native protein, except that cultures were grown in MOPS medium (EZ Rich Defined Medium, Teknova), with SeMet replacing Met. Mutant *Sa*CoADRs (Y361F, Y419F, and the Y361,419F double mutant) and CoADR-RHDs (C44S and C514S) were generated as described for *Ba*CoADR (*20*), using the respective wild-type expression

[2]A. Claiborne, unpublished observations.

Table 1: Data Collection Statistics for *Ba*CoADR-RHD

	MAD[a]				synchrotron reduction[c]	
	edge	peak	remote	LAB[b]	SYNC1	SYNC6
wavelength (Å)	0.9777	0.9774	0.9500	1.5418	0.9790	0.9799
space group		$P2_1$		$P2_1$	$P2_1$	$P2_1$
cell dimensions						
a (Å)		66.91		67.48	67.37	67.62
b (Å)		109.81		110.47	110.47	110.55
c (Å)		79.70		79.99	80.02	80.08
β (deg)		101.55		101.69	101.87	101.84
resolution (Å)	2.00	2.00	2.00	2.10	1.94	2.10
no. of reflections	553706	548558	554389	480091	290767	494031
no. of unique reflections	149500	150035	150510	66422	83942	132117
completeness (%)	99.9 (100)[d]	99.9 (100)	99.8 (99.4)	99.3 (92.5)	99.1 (98.2)	99.8 (100)
R_{merge} (%)	7.0 (36.3)	6.9 (33.3)	7.1 (35.8)	9.7 (30.2)	8.7 (37.2)	9.0 (41.4)
I/σ	10.7 (3.0)	10.7 (3.2)	10.5 (3.0)	33.6 (7.5)	7.1 (2.3)	7.7 (2.6)

[a]Collected at beamline X12C of the National Synchrotron Light Source using a Brandeis Q4 CCD detector. [b]Collected on a Rigaku Saturn-92 CCD detector using Cu Kα radiation from a MicroMax-007 rotating anode X-ray generator. [c]Collected at beamline X26C of the National Synchrotron Light Source using an ADSC Quantum-4 CCD detector. [d]Numbers in parentheses represent data for the highest-resolution shell.

plasmids as templates. Yields for native and mutant CoADR-RHDs and for the SeMet enzyme were 8 and 5 mg/L, respectively.

Kinetic Assays and Anaerobic Titrations. CoADR activities for wild-type and mutant *Sa*CoADRs and CoADR-RHDs were measured as described recently for *Ba*CoADR (*20*), using a Cary 50 spectrophotometer (Varian) thermostated at 25 °C. MMTS-dependent turnover (*26*) was measured at 340 nm in a total volume of 1 mL containing 50 mM potassium phosphate (pH 7.0), 0.5 mM EDTA, 32 μM NADH [which is at least 30 × K_m(NADPH) for *Sa*CoADR reduction of CoAD (*19*)], and 1 mM MMTS, with a final CoADR-RHD concentration of 20 nM. DTNB-dependent turnover was measured identically, except that 200 μM DTNB replaced MMTS, and 5-thio-2-nitrobenzoate (TNB) product formation was monitored at 412 nm (*27*). Steady-state kinetic parameters for MMTS-dependent turnover with *Sa*CoADR and CoADR-RHD were determined from initial velocity measurements taken with the Applied Photophysics DX.17 MV stopped-flow spectrophotometer, with final enzyme concentrations of 100 nM. MMTS concentrations were varied over the range of 0.01−1.5 mM, at a fixed NAD(P)H concentration of 32 μM. Initial rates were linear for at least 4 s (CoADR-RHD) or 6 s (*Sa*CoADR, 33% of the total ΔA_{340}); all measurements were repeated six times and were corrected for NAD(P)H oxidase activities measured in parallel, and kinetic data were analyzed as recently described for *Ba*CoADR (*20*).

Extinction coefficients for wild-type and C514S CoADR-RHD proteins (ε_{451} = 12000 and 11900 M^{-1} cm^{-1}, respectively) were determined by standard methods (*19*). An extinction coefficient for reduced wild-type *Ba*CoADR-RHD (ε_{451} = 1200 M^{-1} cm^{-1}) was assumed, on the basis of the extinction coefficient determined experimentally for dithionite-reduced *Ba*CoADR (*20*). Anaerobic titrations followed established protocols (*20*), using a Hewlett-Packard model 8452A diode array spectrophotometer.

CoADR-RHD Crystal Preparation and Data Collection. SeMet CoADR-RHD was used for all crystal preparation and data collection. Thawed aliquots of SeMet CoADR-RHD were concentrated to 7 mg/mL in 10 mM sodium *N*-(2-hydroxyethyl)piperazine-*N*′-2-ethanesulfonic acid (pH 7.2), and 4 mM NAD^+ was added. Large, single crystals grew in 4 μL + 4 μL sitting drops over reservoirs of 0.5 mL of 8−16% PEG8000, 2% (v/v) 2-methyl-2,4-pentanediol, and 0.2 M potassium acetate (pH 6.0) at 15 °C. These crystals were harvested and crushed before streak seeding (*28*) to fresh drops in plates that had been equilibrated overnight. Crystals grew to full size in 1−2 weeks; prior to data collection, they were soaked in 18−20% PEG8000, 15−20% 2-methyl-2,4-pentanediol, and 0.2 M potassium acetate (pH 6.0) and flash-frozen in a nitrogen stream at 100 K. An oxidized (Cys44-SSCoA) CoADR-RHD data set was collected in-house on a Rigaku Saturn-92 CCD detector using Cu Kα radiation from a MicroMax-007 rotating anode X-ray generator and processed using HKL2000 (*29*). A three-wavelength data set for MAD phasing was collected with a single SeMet CoADR-RHD crystal at beamline X12C of the National Synchrotron Light Source and indexed, integrated, and scaled using d*TREK (*30*). For synchrotron reduction experiments, another SeMet CoADR-RHD crystal was used to collect six complete data sets (in the order *peak1*, *remote1*, *inflection1*, *peak2*, *remote2*, and *inflection2*) at beamline X26C of the National Synchrotron Light Source. These data sets were also indexed, integrated, and

Table 2: Crystallographic Refinement Statistics for Oxidized and Synchrotron-Reduced SeMet CoADR-RHD Structures

	LAB	SYNC1	SYNC6
resolution range (Å)	42.56−2.10	39.16−1.94	46.13−2.10
amplitude cutoff	none	none	none
no. of amino acid residues	1109[a]	1109	1110
no. of waters	665	730	271
no. of total non-hydrogen atoms	9469	9559	9098
R-factor (%)	17.4	18.3	21.3
R_{free} (%)	21.8	22.8	25.5
stereochemical ideality			
bond length rmsd (Å)	0.010	0.009	0.011
bond angle rmsd (deg)	1.3	1.3	1.4
φ and ψ most favored (%)	91.6	92.3	91.7
φ and ψ additional allowed (%)	8.1	7.2	7.8
φ and ψ generously allowed (%)	0.1	0.3	0.3

[a]The number of amino acid residues corresponds to the CoADR-RHD dimer and includes residues of the N-terminal His tag that were modeled in the final structures.

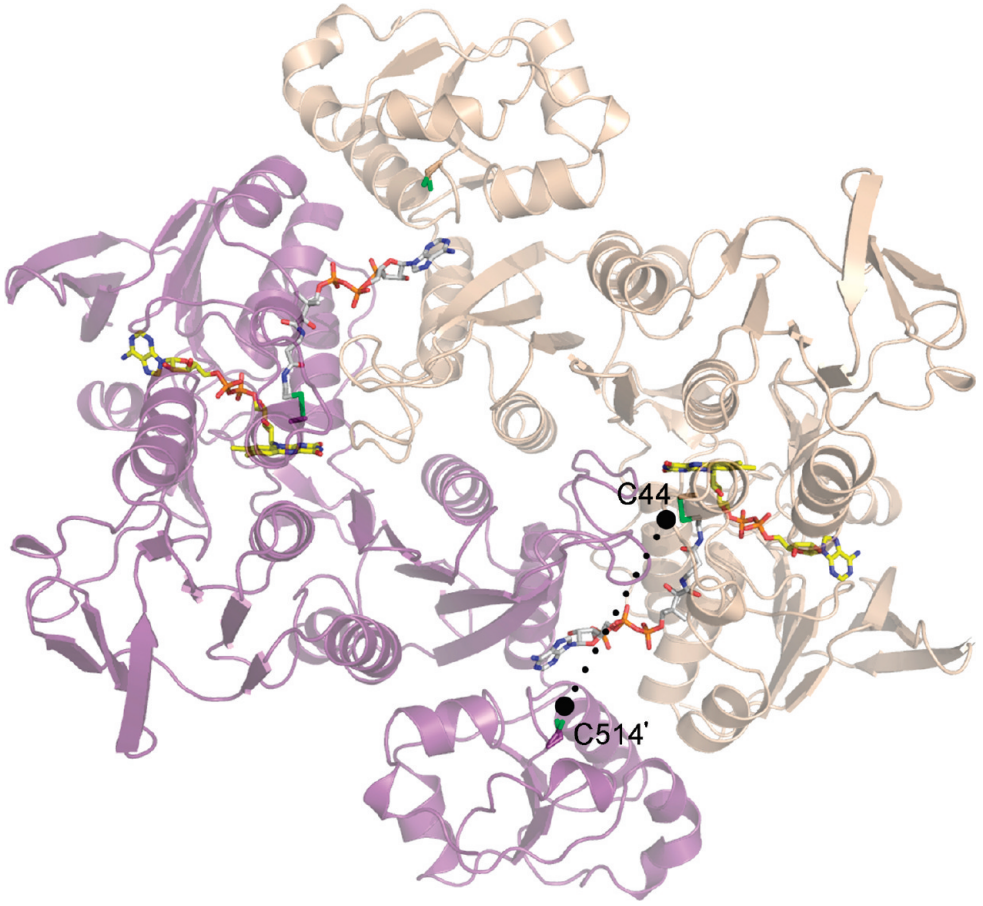

FIGURE 1: Oxidized *Ba*CoADR-RHD dimer, colored by subunit: chain A, wheat; chain B, purple. FAD, CoAS−, and Cys-S_γ are color-coded by atom type, with carbon atoms colored yellow for FAD and white for CoAS−. Cys44, the active-site Cys of the CoADR module, and Cys514′, the active-site Cys of the RHD, are labeled in chains A and B, respectively. A dotted black line connects the two Cys-S_γ atoms. Secondary structure is rendered as 50% transparent.

scaled using d*TREK. Table 1 summarizes data collection statistics for the MAD phasing, in-house (LAB), and *peak1* (SYNC1) and *inflection2* (SYNC6) data sets that were used in the structure determinations.

CoADR-RHD Phasing and Structure Refinement. Using the MAD data set, 31 of 34 Se sites per dimer were located using SOLVE (*31*). These heavy atom positions were refined, and initial phases were calculated using MLPHARE (*32*). Manual inspection of difference map peaks allowed identification of two more Se sites, and these were included in subsequent SOLVE calculations. Density modification and automatic building with RESOLVE (*33*, *34*) allowed 77% of the dimer to be built, and the remaining residues, FAD, and CoAS− were built manually with *O* (*35*). Refinement was conducted at 2.0 Å resolution using CNS (*36*) with rounds of manual rebuilding, simulated annealing, energy minimization, and individual *B*-factor refinement. Water molecules were identified using a 3σ difference Fourier cutoff. Multiple rounds of refinement in CNS resulted in an *R*-factor of 17.6% and an R_{free} of 22.3% for SeMet CoADR-RHD (data not shown).

Because partial reduction of the active-site disulfide was observed, this structure was not used for structural interpretation. This structure was used to determine the oxidized (Cys44-SSCoA) CoADR-RHD structure by molecular replacement using the LAB data set. Initial rounds of refinement were conducted in CNS; final rounds were performed using TLS (*37*) plus restrained refinement in REFMAC5 (*38*), with manual rebuilding in COOT (*39*). Waters (in $2F_o - F_c$ peaks greater than 1σ) were added to the structure using COOT. The SYNC1 and SYNC6 synchrotron-reduced CoADR-RHD structures were determined using the final oxidized CoADR-RHD structure as the molecular replacement model. The final SYNC1 and SYNC6 structures were refined using TLS plus restrained refinement in REFMAC5. Refinement statistics for all three models (LAB, SYNC1, and SYNC6) are summarized in Table 2.

Structure superpositions and sequence alignments were performed using DALI (*40*), DALILITE (*41*), and COOT (*39*), and CLUSTALW (*42*), DIALIGN (*43*), and ESPript (*44*), respectively. Figures of protein molecules and residues were prepared using PyMOL (*45*).

Mass Spectrometry and Limited Proteolysis. ESI-TOF mass spectrometric analysis was conducted with an Agilent MSD TOF system. The operating conditions for mass spectrometric analysis were recently described by Jönsson et al. (*46*), except the fragmentor voltage was 360 V. Sample injection and data analysis protocols were also recently described (*46*). Reactions (100 μL) including 60 μM wild-type CoADR-RHD, with varying concentrations of NADH and MMTS, in 50 mM potassium phosphate (pH 7.0) and 0.5 mM EDTA were initiated at room temperature by addition of NADH. NADH and MMTS concentrations were varied (at an [MMTS]/[NADH] ratio of 1.5−2) to provide for 0, 10, and 100 turnovers, with NADH as the limiting substrate. After a ca. 1 min incubation, each sample was applied to a Bio-Gel P6 spin column to remove small molecules and subjected to buffer exchange into 50 mM ammonium bicarbonate (pH 8.0).

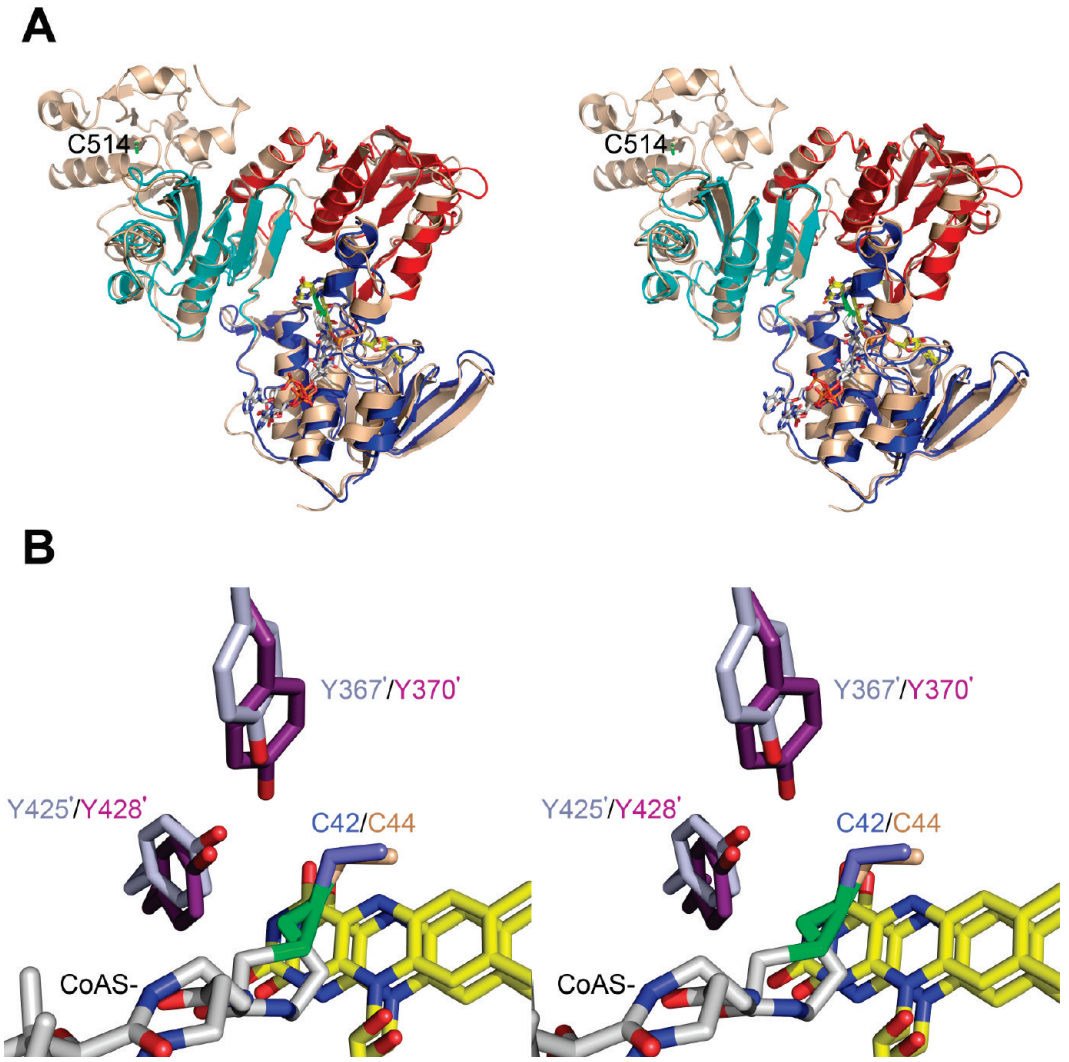

FIGURE 2: Structural comparisons of *Ba*CoADR and *Ba*CoADR-RHD. (A) Superposition, in stereo, for CoADR-RHD chain A (wheat) and a *Ba*CoADR monomer. The *Ba*CoADR monomer is color-coded by domain: blue for the FAD-binding domain, red for the NAD(P)H-binding domain, and cyan for the interface domain. FAD, Cys-S_γ, and CoAS− are color-coded as in Figure 1, and the active-site Cys514 of the RHD is labeled. The superposition was performed with the respective dimers; COOT gives an rmsd of 1.4 Å for 865 C_α atoms. (B) CoADR active-site overlay, in stereo, for CoADR-RHD chain A and *Ba*CoADR. The superposition was performed as described for panel A. FAD and CoAS− (portions removed for the sake of clarity) are color-coded as in Figure 1; C_α and side chain carbon atoms are colored wheat and purple for CoADR-RHD chains A and B, respectively, and slate blue and light blue for *Ba*CoADR chains A and B, respectively. Cys-S_γ is also color-coded as in Figure 1.

Reactions (500 μL) including 5 μM wild-type CoADR-RHD and 15 mM NADH and MMTS (sufficient for 3000 turnovers), in the pH 7.0 phosphate buffer given above, were initiated by addition of enzyme at room temperature. For analysis by limited proteolysis (*47*), native oxidized CoADR-RHD (1:50 trypsin:enzyme, w/w) and CoADR-RHD after 3000 turnovers (1:500 trypsin:enzyme) were incubated in 100 μL of 50 mM Tris-SO_4^{2-} (pH 8.0) and 1 mM $CaCl_2$ at 4 °C for 1 h and for 30 min, respectively. Reactions were quenched via addition of EDTA to a final concentration of 4 mM, and samples were analyzed by sodium dodecyl sulfate−polyacrylamide gel electrophoresis (SDS−PAGE).

RESULTS

Overall Structure of BaCoADR-RHD. Well-diffracting crystals of SeMet-containing *Ba*CoADR-RHD were used to determine the structure by MAD phasing. Since the Cys44-SSCoA disulfide was partially reduced by synchrotron radiation in this structure, we collected data using a laboratory X-ray source to obtain the unperturbed oxidized structure at 2.1 Å resolution. This *Ba*CoADR-RHD model includes residues Ser2−Tyr554 for both chains A and B of the biological dimer (there is one dimer in the asymmetric unit), two FAD cofactors, two covalently bound CoAS− molecules, and 665 solvent waters, all with reasonable geometry (Table 2 and Figure 1). Residues from chain B are designated by a prime symbol. Electron density is also present for the main chain of two residues from the N-terminal His tag (modeled as Gly0 and Gly1) in chain A and one residue in chain B (Gly1′). There is also weak electron density for the ADP moiety of NAD^+ in both subunits, but modeling of these positions results in *B*-factors of >100 Å^2; therefore, they are not included in the final model. Some uninterpreted electron density is also observed near the active-site Cys514 of the RHD (see below). Although noncrystallographic symmetry restraints were not used in refinement, the A and B chains superimpose well, with a C_α root-mean-square deviation (rmsd) of 0.5 Å. Each monomer consists of a CoADR module (residues 2−451) linked to a C-terminal RHD (residues 455−554), with the RHD′ domain (chain B) packing against the CoADR module of chain A (Figure 1).

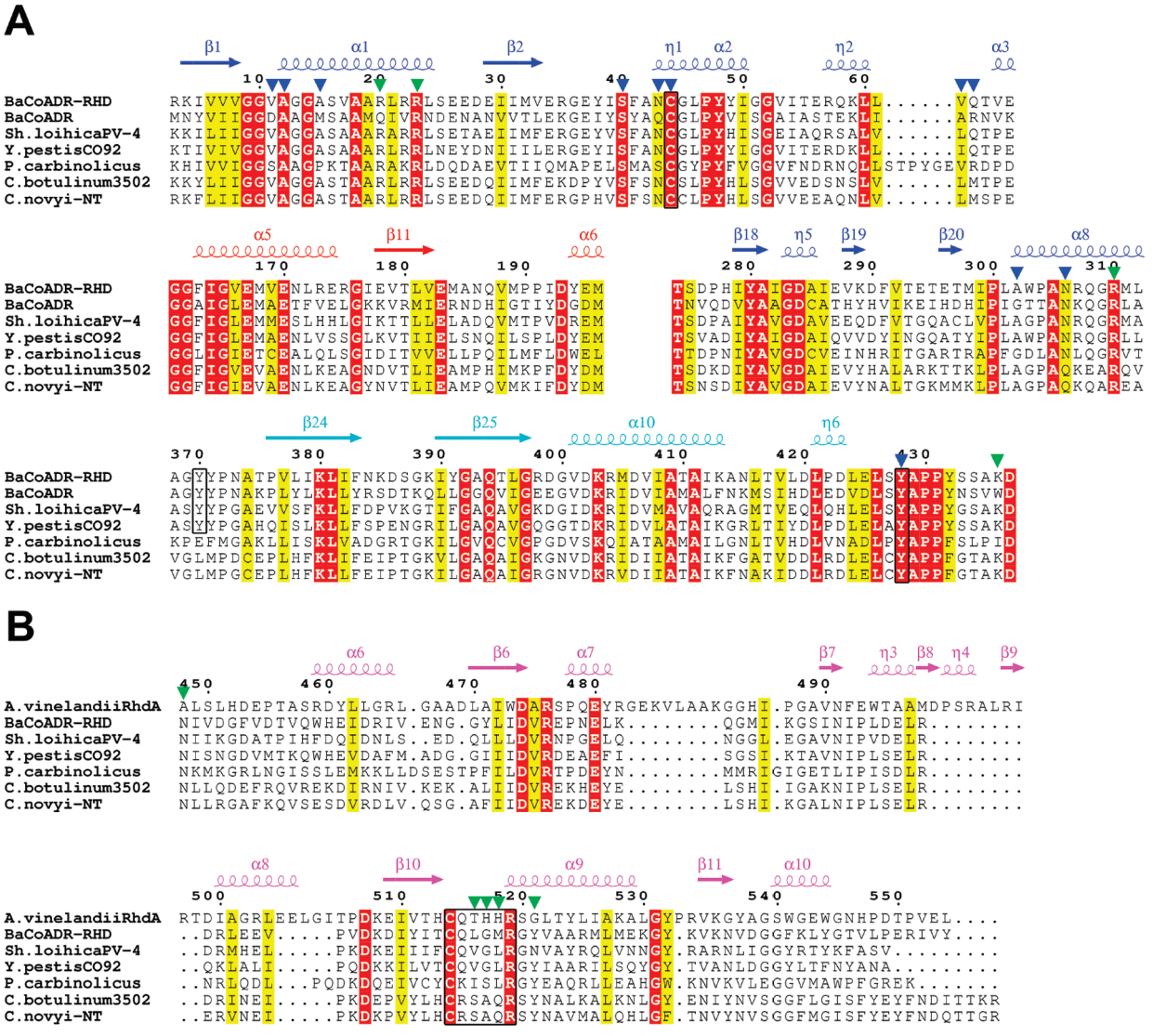

FIGURE 3: (A) Structure-based sequence alignment for *Ba*CoADR-RHD, *Ba*CoADR, and the CoADR modules of CoADR-RHDs from *Sh. loihica* PV-4 (YP_001092860), *Yersinia pestis* CO92 (CAL21605), *P. carbinolicus* (YP_356993), *C. botulinum* ATCC 3502 (CBO1580), and *C. novyi-NT* (YP_878806). The residue numbering corresponds to that of *Ba*CoADR-RHD; conserved residues (red) and conservative substitutions (yellow) are highlighted. The five sequence blocks correspond to FAD-binding-1 (3−66), NADH-binding (161−196), FAD-binding-2 (274−312), and interface (368−437) domain segments, and the active-site Cys44, Tyr370, and Tyr428 (black boxes). Secondary structure assignments (color-coded by domain as for *Ba*CoADR in Figure 2A, with η representing 3_{10}-helical segments) correspond to *Ba*CoADR-RHD. (B) Structure-based sequence alignment for the *A. vinelandii* RhdA rhodanese catalytic domain [residues 140−271; the beginning of the second domain is Glu146 (*53*)] and the RHDs of *B. anthracis*, *Sh. loihica*, *Y. pestis*, *P. carbinolicus*, *C. botulinum*, and *C. novyi-NT* CoADR-RHDs given in panel A. The residue numbering corresponds to that of *Ba*CoADR-RHD, and secondary structure assignments (magenta) correspond to RhdA. The black box represents the C[Q/K/R]*xxx*R catalytic loop. RhdA segments of residues 176−183, 200−209, and 216−218 are absent in the RHDs (see Figure 4A). For both panels, green and blue triangles denote residues from *Ba*CoADR-RHD that interact with the adenosine 3′-phosphate 5′-pyrophosphate and pantetheine moieties, respectively, of CoAS− (see Figure 5A). This alignment was deduced using DALILITE (*41*), DIALIGN (*43*), and ESPript (*44*), together with structural superpositions. Residues Glu557−Leu566 have been omitted from the two clostridial sequences for the sake of clarity.

CoADR Module. A structural superposition of the *Ba*CoADR-RHD and *Ba*CoADR (*20*) dimers shows them to be quite similar [C_α rmsd = 1.4 Å over 865 residues (Figure 2A)], consistent with their 35% sequence identity. Figure 3A gives a partial structure-based sequence alignment for *Ba*CoADR and the CoADR modules of six bacterial CoADR-RHD proteins, including the *B. anthracis* enzyme. The domain structures are the same (Figure 3A, legend), and the largest structural difference involves *Ba*CoADR-RHD residues Glu183−Pro190, a loop that in *Ba*CoADR (Glu180−Thr187) changes conformation on NAD(P)H binding (*20*). In *Ba*CoADR-RHD, these residues are well-ordered and adopt a conformation similar to that observed in the *Ba*CoADR−NAD(P)H complex, suggesting that the conformational change observed in *Ba*CoADR on binding NAD(P)H is not required for CoADR-RHD. In contrast to the NADPH-specific *Sa*CoADR (*16*) and the dual-specificity *Ba*CoADR, the conservation of Gly165 and Glu183 in the CoADR-RHDs (Figure 3A) suggests a marked preference for NADH. We have recently observed (*20*) that *Ba*CoADR Ala160 replaces the active-site Tyr conserved in all known functional GRs (e.g., Tyr197 in human GR), in NADH peroxidase, and in all known functional NADH oxidases. In human GR, the reductive half-reaction was seriously compromised, for example, in the Y197S mutant (*48*). Figure 3A demonstrates that, while the *Pelobacter carbinolicus* CoADR-RHD (*49*) has Leu at the equivalent position, all other enzymes analyzed have Phe. The preference for the

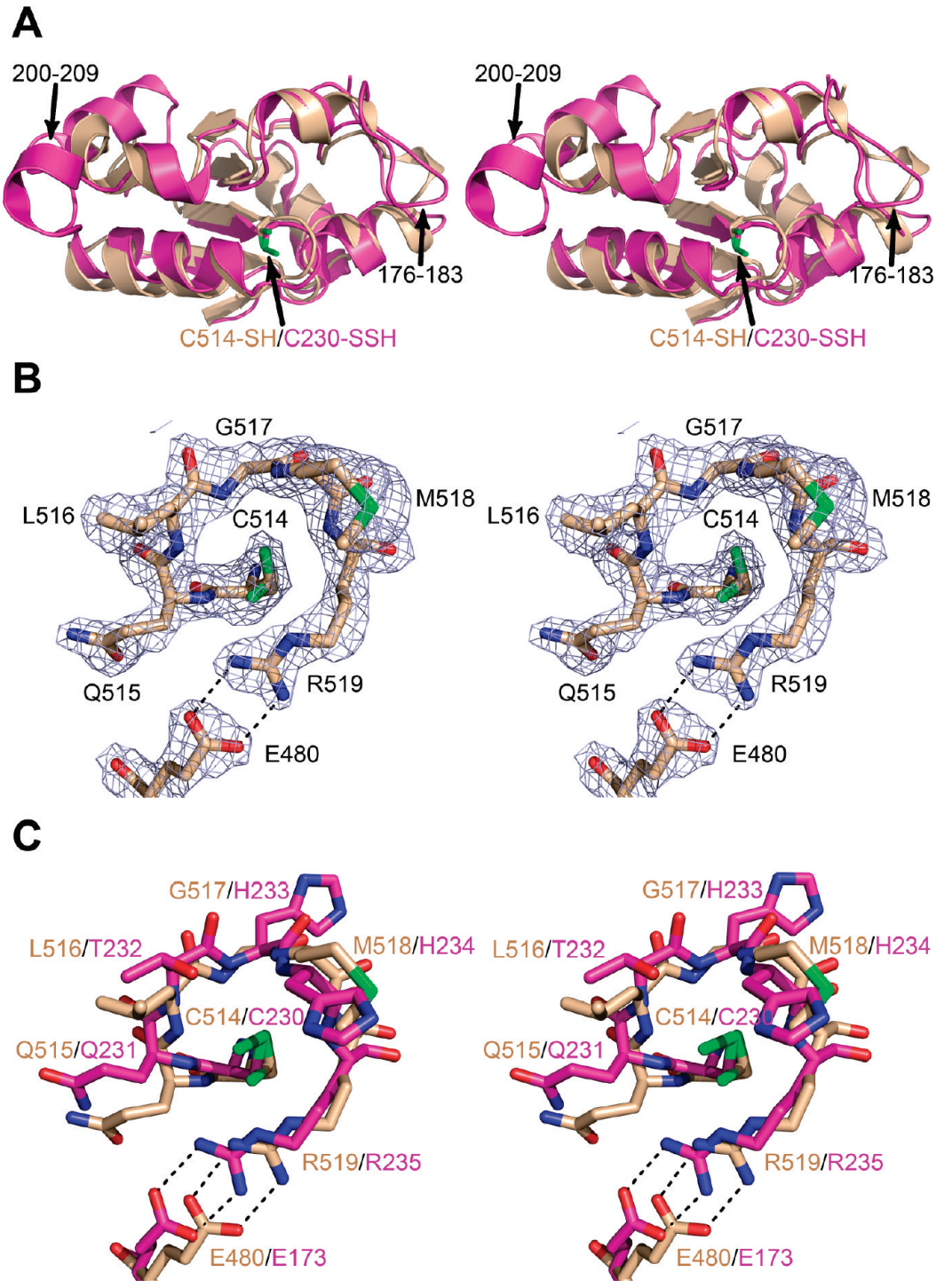

FIGURE 4: Structural comparisons of the RHD of *Ba*CoADR-RHD and the catalytic domain of *A. vinelandii* RhdA rhodanese (PDB entry 1E0C). (A) Superposition, in stereo, of CoADR-RHD residues 455−554 (wheat) and RhdA residues 147−271 (magenta). Cys-S_γ is color-coded as in Figure 1. Arrows indicate two of the RhdA segments that are absent in CoADR-RHD (residues 176−183 and 200−209) as well as the active-site Cys residues of CoADR-RHD (Cys514-SH) and RhdA (Cys230-SSH persulfide). (B) Final $2F_o - F_c$ map, in stereo, for residues Glu480 and Cys514−Arg519 (the CQ*xxx*R catalytic loop of CoADR-RHD), together with the refined model. The depicted contour level is 1σ. The Glu480−Arg519 salt bridge is represented by black dashes. Color-coding is by atom type, with carbon atoms colored wheat; Cys514 is modeled in two distinct side chain conformations. (C) Superposition, in stereo, of the refined model for the RHD catalytic loop of CoADR-RHD as depicted in panel B and the equivalent residues of the RhdA catalytic loop (Glu173 and Cys230−Arg235). Color-coding is by atom type; carbon atoms are colored wheat and magenta for CoADR-RHD and RhdA, respectively. RhdA Cys230 was modeled as a persulfide (*50*).

aromatic side chain as evidenced in the CoADR modules of these enzymes suggests that this residue may play a similar role in covering the *re* face of the flavin in the free enzyme. GR Tyr197 is known to swing out, opening the pocket for the incoming NADPH (*50*); although bound NAD^+ has a limited occupancy in the *Ba*CoADR-RHD structure, with the side chain of Phe163 exhibiting some disorder as well, Phe163 in the refined *Ba*CoADR-RHD model is in the "out" conformation. Figure 3A also demonstrates that the CoADR-RHDs conserve the essential (in *Ba*CoADR and *Sa*CoADR) active-site cysteine (Cys44) as well as one of the two active-site tyrosines (Tyr428′) that play important roles in CoADR catalysis (*20*). The

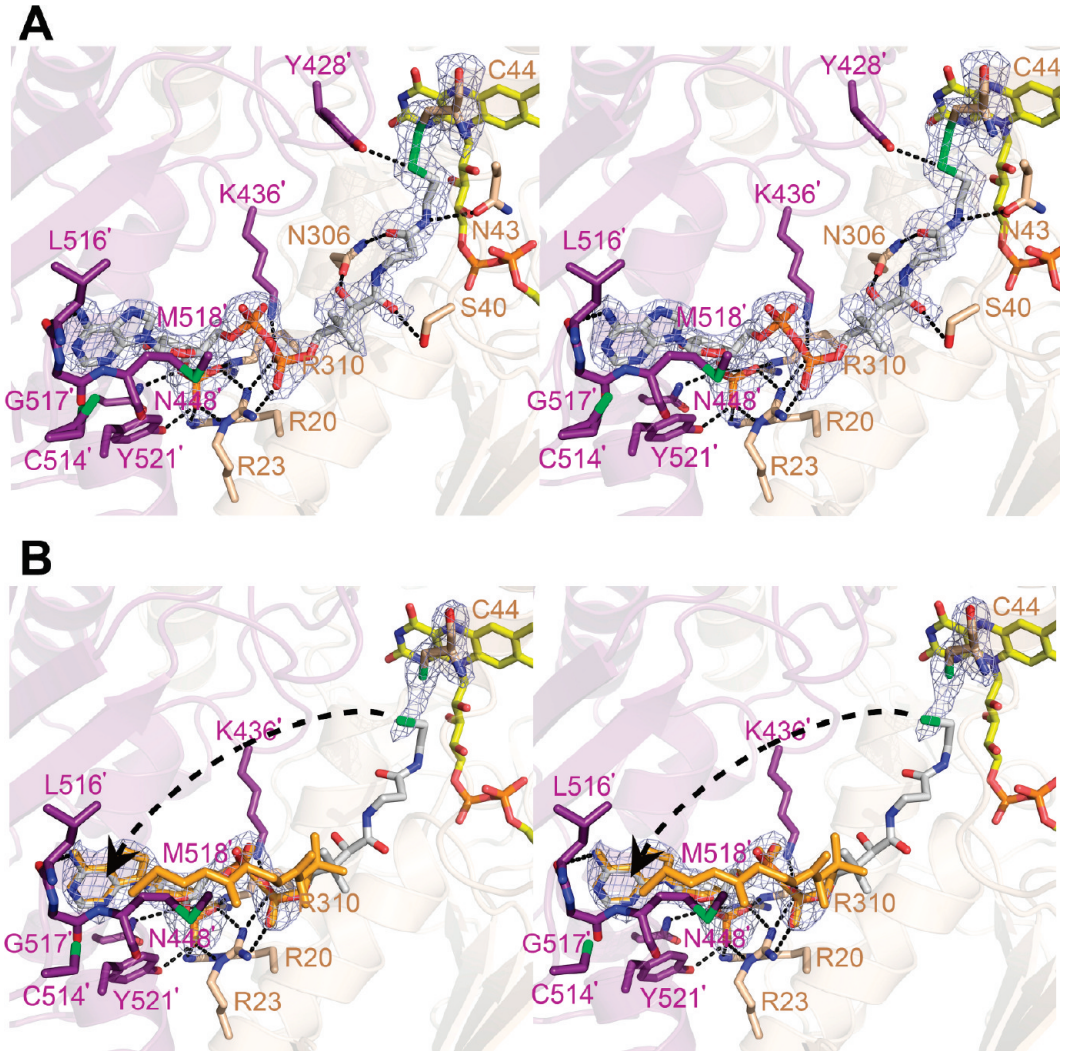

FIGURE 5: CoAS-binding environment and synchrotron reduction of the Cys44-SSCoA center. (A) Stereoview of the Cys44-SSCoA center (chain A) of oxidized CoADR-RHD. The $F_o - F_c$ electron density, contoured at 3σ, was calculated by omitting the Cys44-SSCoA mixed disulfide from the structure and running one round of refinement. FAD (portion removed for the sake of clarity), Cys514′ (both side chain conformations), and residues identified in Figure 3 as providing protein−CoAS contacts are included. FAD, CoAS−, and Cys-S_γ are colored as in Figure 1. C_α and side chain carbon atoms for chains A and B are colored as in Figure 2B. Black dashes represent protein−CoAS hydrogen bonding interactions, and secondary structural elements are rendered as 50% transparent. (B) Same as panel A, but for the synchrotron-reduced SYNC6 structure determination. FAD, Cys44, Cys514′ (now one side chain conformation), and residues providing interactions with the adenosine 3′-phosphate 5′-pyrophosphate component of CoAS− (Figure 3) are still shown. The refined model for the SYNC6 structure includes the full adenosine 3′-phosphate 5′-pyrophosphate component but lacks the pantetheine arm. Using the CoAS− ADP-3′-phosphate as an anchor, a model for the flexible pantetheine arm that reaches to the RHD′ active site was generated by manually adjusting torsion angles. The resulting "bent" CoASH model is colored orange, with a dashed arrow indicating the path of the swinging arm.

P. carbinolicus, *Clostridium botulinum* (*51*), and *Clostridium novyi-NT* (*52*) CoADR-RHDs do not conserve Tyr370 (replaced with Glu, Leu, and Leu, respectively); this is consistent with the earlier observation that while *Ba*CoADR Tyr367′ is not essential for activity, *Ba*CoADR Tyr425′ plays a primary role in protonation of the CoAS-II product during CoAD reduction (*20*).

In the active-site area, *Ba*CoADR-RHD contains a Cys44-SSCoA mixed disulfide in the oxidized structure; similar to *Ba*CoADR, but in stark contrast to *Sa*CoADR (*16*), the CoAS− 3′-phosphate is buried in the protein interior (Figure 1). A notable difference between the non-flavin redox centers (Cys-SSCoA) in *Ba*CoADR and CoADR-RHD is that the respective CoAS-sulfur atoms point in opposite directions (Figure 2B). This is curious given the conserved orientations of the partnering Cys side chains but is reliably determined by the electron density. In CoADR-RHD, this difference facilitates a more favorable interaction between the CoAS-sulfur and Tyr428′-OH (3.2 Å). While *Ba*CoADR-RHD Tyr428′ and *Ba*-CoADR Tyr425′ superimpose very favorably, Tyr370′-OH is shifted 2.2 Å compared to Tyr367′-OH. As a result, CoADR-RHD Tyr370′ is positioned more closely to both the Cys44-SSCoA disulfide and Tyr428′ (Tyr-OH−Tyr-OH distance of only 2.6 Å).

A major difference in CoAS-binding compared with *Ba*-CoADR is that the adenine end of the cofactor is well-buried in *Ba*CoADR-RHD. This occurs, not due to any major change in the interaction within the CoADR module (Figure 2A), but from the position of the RHD′ domain (Figure 1); this will be discussed further below.

Rhodanese Homology Domain. *Ba*CoADR-RHD is the first structural representative of the multidomain proteins class of the rhodanese superfamily (*24*); a DALI search performed on the RHD domain (residues Asp455−Tyr554) identifies the RhdA rhodanese from *A. vinelandii* [rmsd = 1.9 Å, 21% identity (*53*)] as

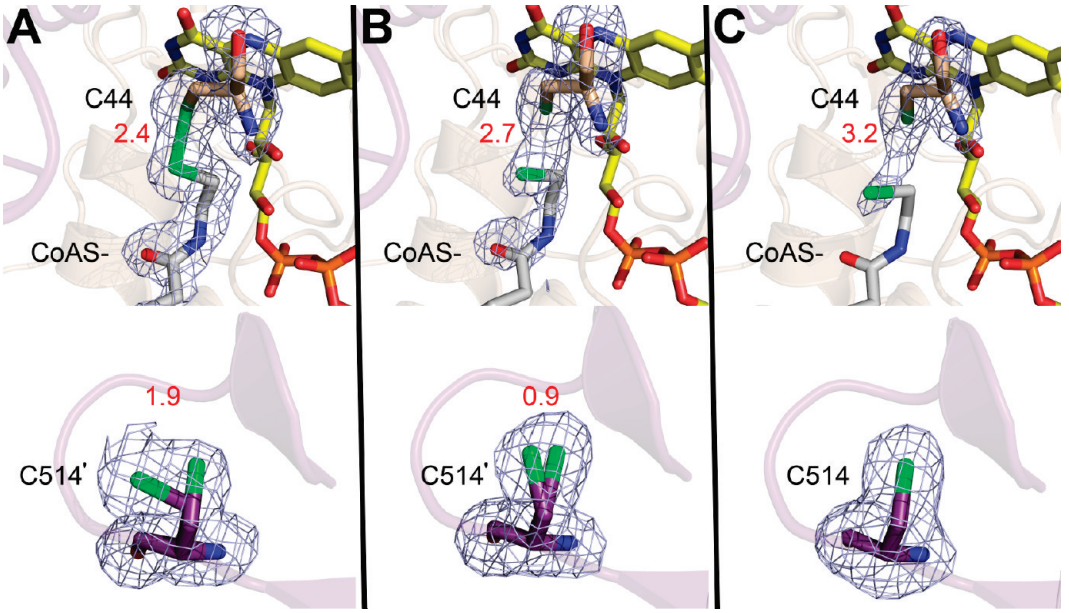

FIGURE 6: Shift in Cys514′ side chain conformer distribution during synchrotron reduction of *Ba*CoADR-RHD. Panels represent $F_o - F_c$ electron density (calculated by omitting Cys44, CoAS−, and Cys514′ from the structures and running one round of refinement) for Cys44, the terminal β-aminoethanethiol moiety of CoAS−, and Cys514′, together with the refined model, for (A) oxidized CoADR-RHD (Figure 5A), (B) the SYNC1 CoADR-RHD structure determined during synchrotron reduction (Tables 1 and 2), and (C) the SYNC6 CoADR-RHD structure determined during synchrotron reduction (Figure 5B). FAD (portion omitted for the sake of clarity) is included in the models. Color-coding for FAD, CoAS−, and Cys-S_γ is as in Figure 1; color-coding for C_α and side chain carbon atoms is as in Figure 2B. Other details are as in Figure 5. Distances (Å) are given in red for Cys44-S_γ−CoAS-sulfur and for Cys514′-$S_\gamma(\alpha)$−Cys514′-$S_\gamma(\beta)$, where α and β represent the two side chain conformers for each refined model.

the most closely related structure among functionally characterized proteins. Figure 3B gives a structure-based sequence alignment for the C-terminal catalytic domain of RhdA (residues 140−271), which contains the active-site Cys230, and the RHD domains of the CoADR-RHD isoforms from Figure 3A. Three segments of RhdA (RhdA residues 176−183, 200−209, and 216−218) are absent in the RHDs (Figures 3B and 4A).

The active-site Cys514 of CoADR-RHD is positioned at the protein surface, 25 Å from Cys44′ of chain B (Figure 1). Cys514 and the whole CQ*xxx*R active-site loop adopt a conformation very similar to that of the RhdA catalytic domain (Figure 4A,C). Cys514-S_γ adopts two conformations (Figure 4B,C), with the stronger one matching the RhdA active-site structure. In addition, a separate superposition (not shown) indicates that RhdA residues Asp200−Thr209 (see above) would clash with a portion of the FAD-binding domain of the CoADR module. This provides a structural basis for understanding the deletion of this segment in the RHD domain of *Ba*CoADR-RHD. Of special interest in the *P. carbinolicus* and clostridial CoADR-RHD sequences (Figure 3B) is the replacement of Gln515 in the CQ*xxx*R loop with a Lys or Arg residue. A similar CK*xxx*R catalytic loop sequence is also seen in the polysulfide-sulfur transferase (Sud) protein from *Wolinella succinogenes* (*54*; see a later section). Krepinsky and Leimkühler (*6*) proposed that the presence of two basic residues in an RHD catalytic loop promotes recognition of thiosulfate ($S{=}SO_3^{2-}$) as a sulfur donor, so this substitution may indicate a shift in the preferred sulfur donor for the *P. carbinolicus* and clostridial proteins.

As noted above, the adenosine 3′-phosphate 5′-pyrophosphate moiety of CoAS− interacts extensively with the RHD′ domain, leading to well-defined binding for the whole Cys44-SSCoA moiety in the oxidized enzyme (Figure 5A). CoAS− is displaced by as much as 4 Å at the adenine relative to the equivalent position in *Ba*CoADR (Figure 2A). The major interactions of adenine with the RHD′ domain (Figure 5A) involve residues Leu516′, Gly517′, Met518′, and Tyr521′ of the RHD catalytic loop. In addition, the CoAS-3′-phosphate interacts with Arg20, Arg23, Arg310, Asn448′, and Tyr521′, while Arg23 and Lys436′ both interact with the CoAS-pyrophosphate. The interactions with the 3′-phosphate and 5′-pyrophosphate elements of CoAS− are similar to those seen in *Ba*CoADR, which binds CoASH tightly enough that it remains in its binding pocket in the reduced *Ba*CoADR−NAD(P)H complexes (*20*). The additional interactions with the RHD′ domain would be expected to anchor it even more firmly.

Synchrotron Reduction of the Cys44-SSCoA Center. To obtain the reduced (Cys44-SH + CoASH) structure of CoADR-RHD, NADH soaks were performed, but the crystals dissolved almost immediately. Since partial Cys44-SSCoA reduction was observed in the structure determined by MAD phasing, we decided to use synchrotron reduction as a tool to produce the reduced form, which has been done by others (*55*, *56*). We collected a series of six complete data sets from a single crystal at the National Synchrotron Light Source and used the first (SYNC1) and sixth (SYNC6) to define partially and fully reduced structures, respectively. Electron density from the SYNC6 data set shows that disulfide reduction has occurred (Figure 5B); we note that the higher *R*-factors (Table 2) and loss of electron density for some side chains [notably, some Asp and Glu carboxylates (data not shown)] also reflect some general crystal damage during the synchrotron reduction experiment.

The adenosine 3′-phosphate 5′-pyrophosphate moiety of CoAS− remains ordered in the SYNC6 structure, but the absence of electron density for the whole pantetheine arm implies that it is flexible within the active site of the reduced enzyme. Berkholz et al. (*56*) reported that synchrotron-reduced structures may not accurately represent a chemically reduced structure, because in the frozen crystal the normal conformational changes

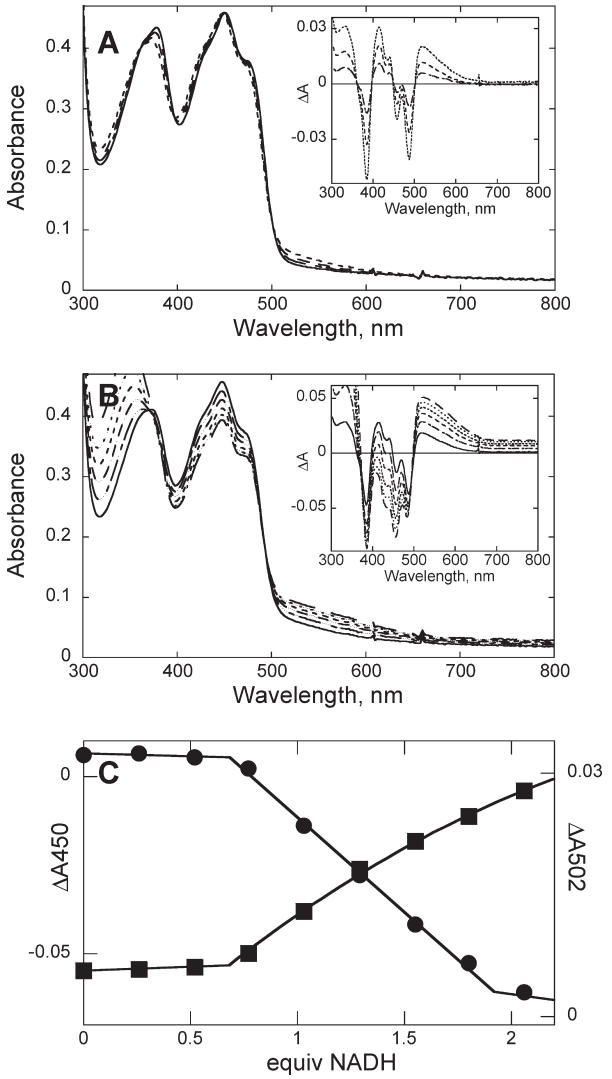

FIGURE 7: Anaerobic titration of wild-type CoADR-RHD with NADH. The enzyme [37.7 μM in 0.75 mL of 50 mM potassium phosphate (pH 7.0) and 0.5 mM EDTA] was titrated with a 5.5 mM solution of NADH. (A) Spectra shown, in order of increasing absorbance at 520 nm, correspond to the addition of 0 (—), 0.26 (−·−), 0.52 (−−−), and 0.77 (···) equiv of NADH/FAD and have been adjusted to zero at 800 nm to correct for an initial baseline shift. The inset shows the difference spectra (minus 0 equiv) shown in order of increasing ΔA_{520} after the addition of 0 (—), 0.26 (−·−), 0.52 (−−−), and 0.77 (···) equiv of NADH/FAD. The difference spectra reveal isosbestic points at 362, 398, 450, and 502 nm. (B) Spectra shown, in order of increasing absorbance at 520 nm, correspond to the addition of 0.77 (—), 1.03 (−·−), 1.29 (−−−), 1.55 (---), 1.80 (···), and 2.06 (— —) equiv of NADH/FAD. The inset shows the difference spectra (minus 0 equiv) shown in order of increasing ΔA_{520} after the addition of 0 (—), 0.77 (—), 1.03 (−·−), 1.29 (−−−), 1.55 (---), 1.80 (···), and 2.06 (— —) equiv of NADH/FAD. (C) Plot of absorbance changes at 450 (●) and 502 (■) nm (see insets for panels A and B) vs the amount of added NADH. The end point for the first phase, taken from the isosbestic points at both 450 and 502 nm, is 0.68 equiv of NADH/FAD; the end point for the second phase, taken from absorbance changes at 450 nm, is 1.92 equiv of NADH/FAD.

associated with disulfide reduction may be inhibited. Thus, the changes seen here may be an underestimate of the changes that would occur in solution, but should not be an overestimate. This strengthens our conclusion that when the disulfide is opened, the whole pantetheine arm does become mobile.

This disordering, and the proximity of the CoAS− adenine to the RHD active site, led us to consider the possibility that the

Scheme 3: Reductive Intermediates on NADH Titration of *Ba*CoADR-RHD

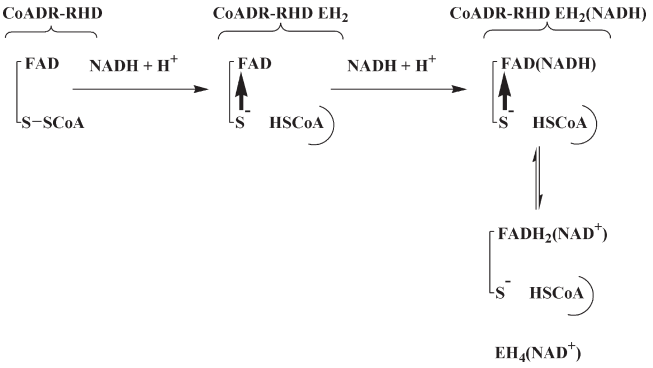

two-electron reduced form of *Ba*CoADR-RHD provides a pantetheine swinging arm that bridges the 25 Å separation between the active-site Cys44 of the CoADR module and Cys514′ of the RHD, with the tight network of electrostatic interactions described above anchoring the reduced CoASH to the protein. As shown in Figure 5B, the conformation of the reduced pantetheine arm can easily be adjusted to a bent form that bridges the gap. This bent form has precedent as it is similar to that observed experimentally in the crystal structure of the *E. coli* pantothenate kinase−CoASH complex [PDB entry 1ESM (*57*)]. Also, there is precedent for pantetheine to serve as a swinging arm. The 4′-phosphopantetheine arm derived from CoASH provides the carrier proteins and intermediate domains in modular polyketide synthases, vertebrate fatty acid synthases, nonribosomal peptide synthases (*58*−*60*), and, now, 10-formyltetrahydrofolate dehydrogenase (*61*), with a ca. 20 Å reach into the active sites of the respective catalytic domains.

The synchrotron-reduced structures also exhibit changes in the RHD active site (Figure 6). In the oxidized form, Cys514′ adopts two distinct conformations for the active-site Cys-S_γ (Figure 6A). The primary conformation matches that reported for RhdA Cys230 in the persulfide (Cys230-SSH) structure [Figure 4C (*53*)], and the secondary one has an uninterpreted peak of extra density associated with it. While we did very carefully evaluate the possibility that the secondary Cys514′-S_γ position in the oxidized form represents a persulfide sulfur, the distance from the Cys514′ sulfur atom (the primary Cys514′-S_γ conformation) to the closest point of the extra density is well > 3 Å, indicating the absence of any covalently bonded atom in this position. The density is continuous, but we have not been able to interpret it.[3] In contrast, in the SYNC6 structure (Figure 6C), only the primary Cys514′ conformation remains, and the additional uninterpreted density has also disappeared. Other than those changes described previously that are thought to reflect crystal damage in this experiment, the movements of Cys44, CoAS(H), and Cys514′ represent the only major differences in the SYNC6 structure.

Redox Properties of CoADR-RHD. Lukose et al. (*17*) have recently reported that anaerobic titration of *Sh. loihica* PV-4 CoADR-RHD resulted in ca. 50% flavin reduction with 5 equiv of NADH/FAD. Examination of the spectral course of that titration indicates the presence of an isosbestic point at 350 nm over the titration phase of 0−2.1 equiv of NADH/FAD, demonstrating the absence of excess NADH. Figure 7 gives the spectral course of an anaerobic NADH titration with

[3]Brito et al. (*12*) reported a similar peak of uninterpreted density near Cys350 in the archaeal sulfide:quinone oxidoreductase structure.

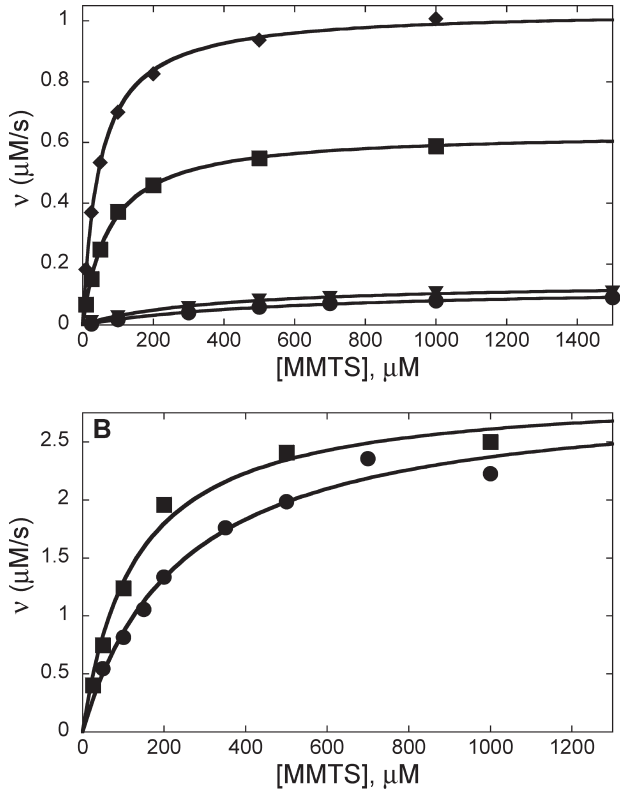

FIGURE 8: Kinetic analyses of MMTS reduction by *Sa*CoADR and *Ba*CoADR-RHD. (A) Primary plots of v (units of μM s^{-1}) vs [MMTS] are presented for wild-type *Sa*CoADR (■) and Y361F (◆), Y419F (●), and Y361,419F (▼) *Sa*CoADR mutants. Initial velocity measurements were performed with the stopped-flow spectrophotometer (see Experimental Procedures). (B) Primary plots of v (units of μM s^{-1}) vs [MMTS] are presented for wild-type CoADR-RHD (■) and the C514S mutant (●). The protocol for these initial velocity measurements followed that described for *Sa*CoADR in panel A, except that 32 μM NADH was used in the assay, replacing NADPH. Although wild-type CoADR-RHD does exhibit inactivation during MMTS reduction in the standard spectrophotometric assay (Figure 9), initial rates of ΔA_{340} remained linear for at least 4 s in the stopped-flow assay.

*Ba*CoADR-RHD. The first phase of the titration [0−0.8 equiv of NADH/FAD (Figure 7A)] does not result in flavin reduction, and the difference spectra indicating maxima at 412 and 518 nm reflect the reduction of Cys44-SSCoA and the appearance of a weak Cys44-S^- → FAD charge-transfer intermediate (*20*). Isosbestic points at 362, 398, 450, and 502 nm confirm the oxidation of all NADH and the absence of any E($FADH_2$) component. Figure 7C represents the first phase as a lag in the absorbance change at both 450 and 502 nm. The second phase of the titration [0.8−2.1 equiv of NADH/FAD (Figure 7B)] gives a further increase in absorbance over the range of 500−800 nm, which accompanies substoichiometric flavin reduction. It is also clear that excess NADH accumulates, beyond 1 equiv/FAD added. Overall, this redox system (Scheme 3) resembles that described previously for NADH peroxidase (*62*), another representative of the NADH peroxidase/oxidase and CoADR subgroup within the two dinucleotide binding domains flavoproteins superfamily (*14*), also group 3 of the flavoprotein disulfide reductase family (*15*). The EH_2 intermediate exhibits none of the redox asymmetry documented recently for *Ba*CoADR (*20*) and differs from that described for NADH peroxidase primarily in the intensity of the 520 nm charge-transfer band. The second phase of the CoADR-RHD redox scheme consists of an equilibrium between static EH_2(NADH) and $EH_4(NAD^+)$ complexes, where the latter intermediate is characterized by a decrease in A_{450} and an increase in absorbance beyond 650 nm. Only partial flavin reduction continues to be observed at up to 14 equiv of NADH/FAD, indicating that the EH_2(NADH) species is favored thermodynamically in this system. At 2.1 equiv of NADH/FAD, only ca. 17% flavin reduction is evident; even at 14 equiv of NADH/FAD, only ca. 27% of the flavin appears to be reduced.

Table 3: Kinetic Parameters for MMTS Reduction with Wild-Type and Mutant Forms of *Sa*CoADR and *Ba*CoADR-RHD

enzyme	K_m^{app}(MMTS) (μM)	k_{cat}^{app} (s^{-1})	k_{cat}/K_m^{app}(MMTS) (M^{-1} s^{-1})
wild-type *Sa*CoADR[a]	78	6.4	8.2×10^4
Y361F *Sa*CoADR	47	10.4	2.2×10^5
Y419F *Sa*CoADR	575	1.2	2.1×10^3
Y361,419F *Sa*CoADR	346	1.4	4.0×10^3
wild-type CoADR-RHD	130	29	2.2×10^5
C514S CoADR-RHD	244	29	1.2×10^5
C44S CoADR-RHD		0	

[a]The *Sa*CoADR Y361F, Y419F, and Y361,419F mutants give apparent turnover numbers of 2 s^{-1} (7%), 5 s^{-1} (19%), and 0, respectively, in the standard CoAD reduction assay, relative to wild-type enzyme (27 s^{-1} = 100%).

MMTS as an Alternate Disulfide Substrate. In the standard CoADR assay, *Ba*CoADR-RHD does not catalyze CoAD reduction; the same absence of CoADR activity has been reported for the *Sh. loihica* enzyme (*17*). This could be due to an inability of the bulky CoAD substrate to approach Cys44 of the reduced CoADR-RHD in the proper geometry; alternatively, the single CoASH may remain bound so tightly (Figure 5B and ref *20*) that it cannot be displaced by a new CoAD substrate. To test whether the enzyme is capable of carrying out disulfide reductase chemistry, we assayed the activities of both *Sa*CoADR and *Ba*CoADR-RHD with MMTS. MMTS [$CH_3SSO_2CH_3$ (*63*)] is a small neutral thiol reagent that has been used as an alternate substrate with yeast GR (*26*) and *Plasmodium falciparum* thioredoxin reductase (*64*); both are flavoprotein disulfide reductases within the same superfamily (disulfide reductase subgroup) as CoADR (*14*), also flavoprotein disulfide reductase groups 1 and 2, respectively (*15*). MMTS reduction yields CH_3SH + $CH_3SO_2^-$; for GR, k_{cat}/K_m(MMTS) = 3.7×10^3 M^{-1} s^{-1} (via the interchange Cys), and turnover is accompanied by a relatively slow inactivation process that has been attributed to the parallel reaction of the charge-transfer Cys (*26*).

Figure 8A and Table 3 give the steady-state kinetic parameters for *Sa*CoADR with NADPH and MMTS, determined from stopped-flow initial velocity measurements. With *Sa*CoADR, the wild type [k_{cat} = 6.4 ± 0.1 s^{-1}, and K_m(MMTS) = 78 ± 3 μM], Y361F [k_{cat} = 10.4 ± 0.1 s^{-1}, and K_m(MMTS) = 47 ± 2 μM], Y419F [k_{cat} = 1.2 ± 0.1 s^{-1}, and K_m(MMTS) = 575 ± 41 μM], and the Y361,419F double mutant [k_{cat} = 1.4 ± 0.1 s^{-1}, and K_m-(MMTS) = 346 ± 48 μM] were analyzed. The k_{cat}/K_m(MMTS) for wild-type *Sa*CoADR of 8.2×10^4 M^{-1} s^{-1} represents a 22-fold increase over the value for yeast GR (*26*). Surprisingly, the catalytic efficiency of the *Sa*CoADR Y361F mutant is enhanced 2.7-fold over that of the wild-type enzyme with this alternate substrate and may reflect a preference for the more hydrophobic Phe side chain in stabilizing apolar elements (e.g., CH_3 groups) in either transition state [Cys43-$S^-\cdots S(CH_3)SO_2CH_3$ or $FADH_2\cdots$Cys43-$SSCH_3$ (Scheme 4)] during MMTS reduction. k_{cat}/K_m(MMTS) values for both Y419F and Y361,419F

Scheme 4: Proposed Mechanism for MMTS Reduction by *Sa*CoADR

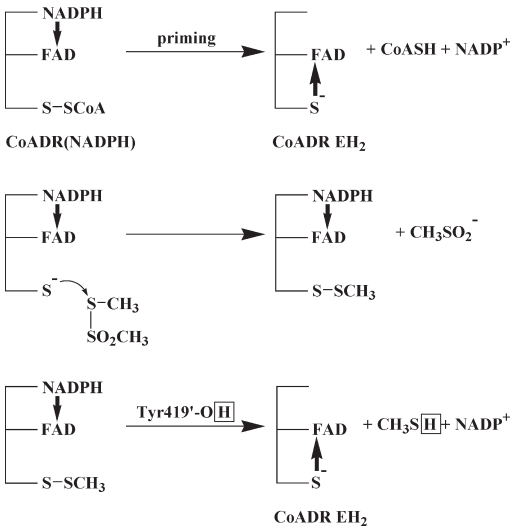

*Sa*CoADR mutants are 2−5% of the wild-type value; these results support the proposed role for Tyr419 in acid−base catalysis,[4] in this case involving protonation of CH_3S^- [pK_a = 10.3 (*65*)] in the reductive half-reaction [Scheme 4; the pK_a of $CH_3SO_2^-$ is 2.3 (*66*)]. The high activity of the Y361F mutant also reinforces the suspicion that the substitution of Leu, or even Glu, for Tyr370 in the clostridial and *P. carbinolicus* CoADR-RHD sequences (Figure 3A) need not be debilitating.

Figure 8B and Table 3 show that wild-type [$k_{cat} = 29 \pm 1$ s^{-1}, and K_m(MMTS) = 128 ± 20 μM] and C514S [$k_{cat} = 29 \pm 2$ s^{-1}, and K_m(MMTS) = 244 ± 34 μM] *Ba*CoADR-RHDs catalyze MMTS reduction with an efficiency [k_{cat}/K_m(MMTS)] 2 times greater than that for wild-type *Sa*CoADR, showing CoADR-RHDs to be catalytically competent for disulfide reduction. As expected, the C44S mutant has no detectable activity, confirming that all MMTS reduction occurs within the CoADR module. In contrast, however, to the linear initial rates observed with the wild-type enzyme in the stopped-flow spectrophotometer, steady-state turnover experiments with the Cary 50 spectrophotometer demonstrated a complete loss of activity over 3 min (Figure 9), similar to but 8-fold faster (at 1 mM MMTS) than the inactivation observed with yeast GR (*26*). The pseudo-first-order rate for inactivation at 1 mM MMTS is 1.6 min^{-1} (Figure 9), and this rate is dependent on MMTS concentration. Parallel analysis of the CoADR-RHD C514S mutant demonstrates that Cys514 of the RHD is required for rapid inactivation. The addition of fresh NADH at this point does not reverse the inactivation, and freshly added wild-type enzyme duplicates the original progress curve, showing that no inhibitory product has accumulated. Also, preincubation of CoADR-RHD with 1 mM MMTS has no effect on the initial rate observed with subsequent NADH addition.

Cys514 Is Essential for Efficient Catalytic Reduction of DTNB. Lukose et al. (*17*) reported that *Sh. loihica* CoADR-RHD catalyzes NADH-dependent DTNB reduction [apparent

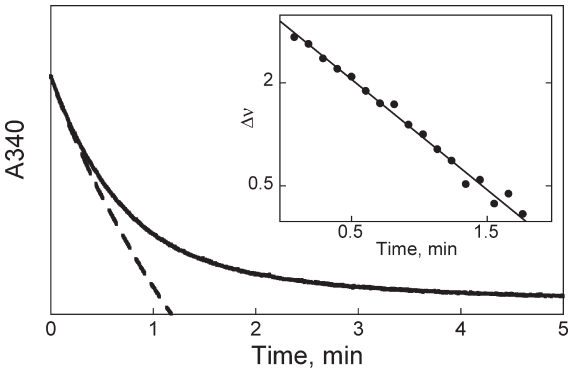

FIGURE 9: Inactivation of wild-type CoADR-RHD during turnover with MMTS. Shown are the time courses for NADH:MMTS oxidoreductase activity with wild-type (—) and C514S mutant (− − −) forms of CoADR-RHD, with 32 μM NADH and 1 mM MMTS. Both reactions were initiated by addition of enzyme and were followed using a Cary 50 spectrophotometer thermostated at 25 °C (see Experimental Procedures). The inset shows semilogarithmic analysis of Δv vs time for wild-type CoADR-RHD during turnover with 1 mM MMTS. Δv was calculated by taking the difference between the observed velocity (μM min^{-1}, measured every 6 s) and the velocity at full inhibition (measured after four half-lives). From this analysis, the pseudo-first-order rate for inactivation is 1.6 min^{-1} at 1 mM MMTS.

K_m(DTNB) = 116 μM, $k_{cat} = 19.9$ s^{-1}, and k_{cat}/K_m(DTNB) = 1.7 × 10^5 M^{-1} s^{-1}]; these steady-state parameters predict a turnover number of 12.6 s^{-1} at 200 μM DTNB and saturating NADH. When wild-type *Ba*CoADR-RHD is assayed in the presence of 32 μM NADH and 200 μM DTNB, a turnover number of 5.2 s^{-1} is observed (data not shown), suggesting that the kinetic parameters for DTNB reduction by the two CoADR-RHDs are similar. In contrast to the results with MMTS, however, there is no turnover-dependent inactivation with DTNB, and the C514S mutant is only ca. 4% as active as the wild-type enzyme. The C44S mutant again has no detectable reductase activity. These results demonstrate that Cys514 is essential for efficient DTNB reduction and suggest that the two Cys-dependent active sites (CoADR and RHD′) communicate during turnover, despite their 25 Å separation in the crystal structures.

The simplest mechanism for this communication is our proposal above that the tightly bound, reduced CoASH functions as a cofactor (Figure 5B) that provides for communication between Cys44 and Cys514′, via a swinging pantetheine arm (Scheme 5). Beginning with the oxidized (FAD, Cys44-SSCoA) wild-type enzyme (species 1 in Scheme 5), DTNB reacts with Cys514′ to give the mixed disulfide (species 2 in Scheme 5). The catalytic loop of the RHD domain has a net positive charge (Arg in position 6), and Krepinsky and Leimkühler (*6*) have described how negatively charged sulfur donors like thiosulfate and 3-mercaptopyruvate interact electrostatically with the respective sulfurtransferase active sites. A similar electrostatic attraction could direct the anionic DTNB substrate to this site, within the RHD domain. In the second step, NADH reduction via the flavin (Scheme 3) yields the EH_2 intermediate (Cys44-SH + CoASH), and the nascent pantetheine-SH arm swings into position, approaching the Cys514′-SSTNB disulfide; subsequent thiol−disulfide exchange gives pantetheine-SSTNB and restores Cys514′-SH (species 3 in Scheme 5). In the penultimate catalytic step, the swinging pantetheine-SSTNB arm delivers the mixed disulfide to the active site of the CoADR module (species 4 in Scheme 5); the final thiol−disulfide interchange with Cys44-S$^-$ restores the resting, oxidized form of the enzyme (species 1).

[4]During anaerobic titration of the *Sa*CoADR Y419F mutant, complete flavin reduction is observed upon addition of 1 equiv of NADPH/FAD; this is commensurate with the appearance of a strong charge-transfer band [E($FADH_2$−$NADP^+$)] centered at 755 nm. This behavior is very distinct from that of wild-type *Sa*CoADR, in which only one FAD per dimer is reduced with NADPH in static titrations, and demonstrates that Tyr419 is paramount to this intrinsic redox asymmetry.

Scheme 5: Proposed Mechanism for Cys514′-Dependent DTNB Reduction by CoADR-RHD[a]

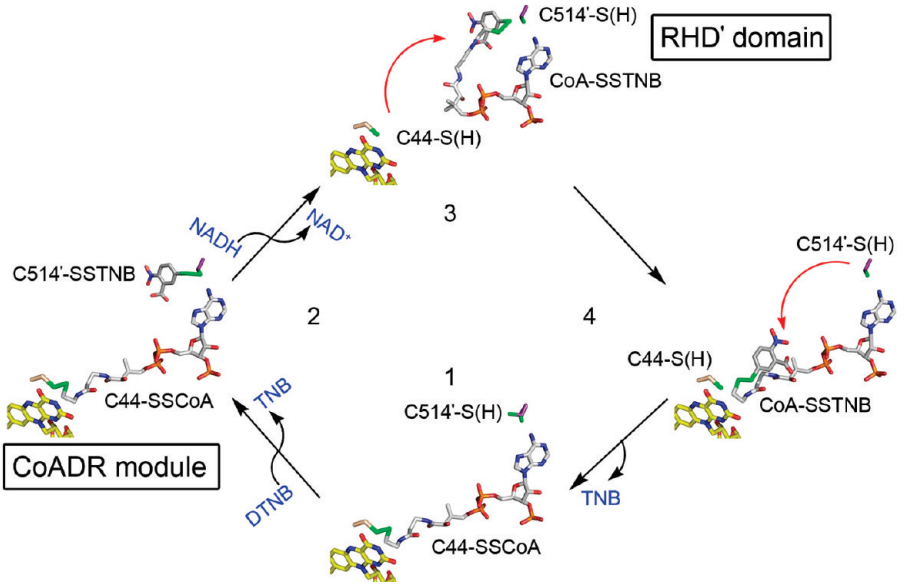

[a]The conversion of enzyme state 2 into state 3 involves reduction of C44-SSCoA, the swing of the pantetheine arm, and the transfer of TNB from C514′ to CoAS−.

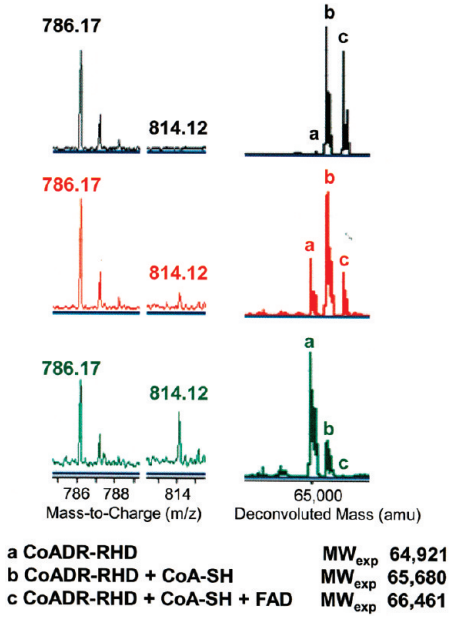

FIGURE 10: ESI-TOF mass spectrometric analyses of wild-type *Ba*CoADR-RHD inactivation during NADH:MMTS oxidoreductase turnover. The three panels give results for 0 (top panel, black), 10 (middle panel, red), and 100 (bottom panel, green) turnovers. The *m*/*z* species identified at 786 and 814 correspond to FAD (calculated *m*/*z* of 785.6 Da) and the asymmetric CoA-SSCH$_3$ (calculated *m*/*z* of 814.6 Da). The deconvoluted protein masses given on the right of each panel correspond to (a) CoADR-RHD [deflavo enzyme lacking CoAS− (*m* = 64921 Da)], (b) CoADR-RHD deflavo enzyme [Cys44-SSCoA form (*m* = 65680 Da)], and (c) CoADR-RHD holoprotein [Cys44-SSCoA form with noncovalent FAD (*m* = 66461 Da)].

The very low (4% of that of the wild type) DTNB reductase activity measured with the C514S mutant may be attributable to a direct but inefficient reaction between the pantetheine-SH and DTNB, but with no catalytic source of pantetheine-SH (the C44S mutant), there is no activity. Nor do we support any scheme involving direct reaction of Cys44 with DTNB (in either the wild type or C514S mutant); this is consistent with the failure of *Sa*CoADR to catalyze DTNB reduction (*67*). Finally, the enzyme would be expected to form a pantetheine-SSCys514′ derivative in the event TNB is displaced instead of Cys514′-SH (species 3). In the absence of a disulfide reductant, the enzyme would be trapped in this catalytically inactive form; such a scenario may have relevance to the inactivation of the wild-type enzyme observed during turnover with MMTS.

To summarize, CoADR-RHD Cys44 is essential for both DTNB and MMTS reductase activities; the respective k_{cat}/K_m values of 1.7×10^5 M^{-1} s^{-1} [*Sh. loihica* CoADR-RHD with DTNB (*17*)] and 2.2×10^5 M^{-1} s^{-1} [*Ba*CoADR-RHD with MMTS (Table 3)] are very similar, both to each other and to the value for *Sa*CoADR with MMTS (8.2×10^4 M^{-1} s^{-1}). Cys514′ of CoADR-RHD is essential for efficient DTNB reduction, but it is not involved in catalytic MMTS reduction. It is required for rapid inactivation during turnover with MMTS, but no inactivation is observed during DTNB reduction.

ESI-TOF Analyses of BaCoADR-RHD Inactivated during MMTS Turnover. We have tested the possibility that a pantetheine-SSCys514′ disulfide is responsible for the inactivation observed during MMTS turnover, using ESI-TOF mass spectrometry. The oxidized wild-type CoADR-RHD (species 1 in Scheme 5) presents two distinct *m*/*z* species by ESI-TOF [Figure 10, top panel (black)]: the holoprotein [*m*/*z* species c; *Ba*CoADR-RHD Cys44-SSCoA form with noncovalent FAD (*m* = 66461 Da)] and the deflavo enzyme without FAD [*m*/*z* species b (*m* = 65680 Da)]. Scheme 6 provides a chemical and structural view of Cys514′-SSCoA formation and inactivation, as proposed. The cycle begins with the *Ba*CoADR-RHD Cys44-SSCH$_3$ intermediate formed in turnover; Cys514′-SH reacts with a second MMTS in a reaction comparable to that described earlier with DTNB. The resulting Cys44-SSCH$_3$, Cys514′-SSCH$_3$ species is common to the two proposed mechanisms of inactivation. In mechanism B, the reduced pantetheine-SH of bound CoASH swings into position approaching the Cys514′-SSCH$_3$ disulfide. The resulting thiol−disulfide exchange gives the Cys514′-SSCoA disulfide, displacing CH_3SH. Formation of this species, during MMTS turnover and inactivation in the absence

Scheme 6: Proposed Mechanisms for Inactivation of CoADR-RHD during Turnover with MMTS[a]

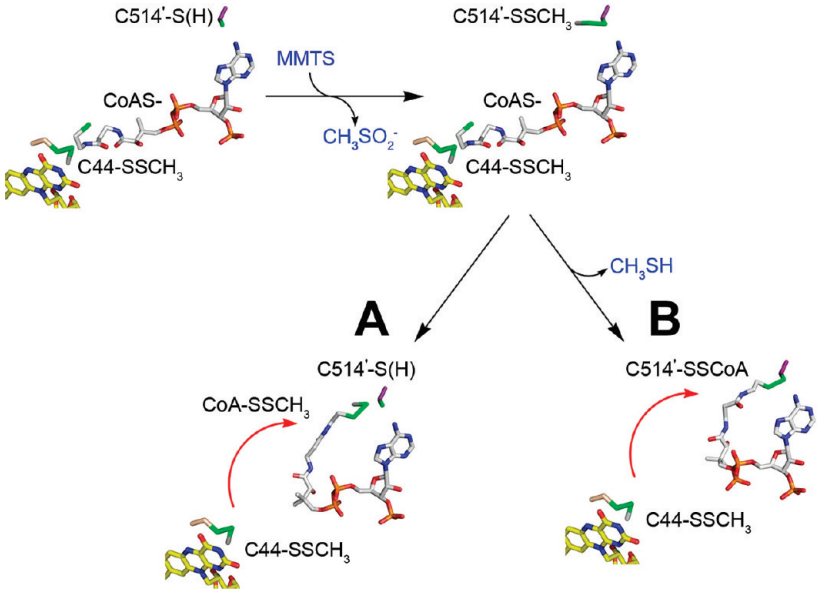

[a]The starting enzyme species has already reacted with NADH and MMTS, resulting in *S*-methylthiolation of C44. This C44-$SSCH_3$ intermediate is not present in the final enzyme form as analyzed by ESI-TOF. Inactivation pathway A involves the swing of the pantetheine arm and the transfer of CH_3S- from C514′ to CoAS−. Pathway B involves the swing of the pantetheine arm, the displacement of CH_3SH, and the formation of the C514′-SSCoA disulfide.

of a disulfide reductant, would also be expected to give *m*/*z* species b and/or c. Figure 10 [middle panel (red) and bottom panel (green)] clearly shows that the levels of both *m*/*z* species decrease with the extent of inactivation. Instead, there is a correlation among the number of catalytic cycles (and increasing enzyme inactivation), reduction in the intensities of *m*/*z* species b and c, and the appearance of a new species a (*m* = 64921 Da), attributed to the loss of CoAS(H) from the deflavo enzyme. This loss of CoAS(H) can occur only via an initial NADH-reduced (Cys44-SH + CoASH) intermediate, as implied in Scheme 6 and as will be discussed below on the basis of preliminary experiments. While there is no *m*/*z* peak corresponding to free CoASH (*m* = 768 Da), there is a commensurate increase in a new low-mass species of 814 Da, in perfect agreement with the mass calculated for CoA-$SSCH_3$. The simple addition of CH_3S- (*m* = 47 Da) to Cys514′ and/or Cys44 should have been detectable, since ESI-TOF instruments routinely achieve measurements with better than 5 ppm accuracy.

We conclude that while the inactivation of CoADR-RHD during turnover with MMTS is not due to accumulation of a Cys514′-SSCoA form, it is correlated with modification of the tightly bound, reduced CoASH cofactor with MMTS; this most likely occurs via the proposed Cys514′-$SSCH_3$ intermediate (Scheme 6, mechanism A). The molecular linkage between CoASH *S*-methylthiolation and the loss of MMTS reductase activity within the CoADR module is currently under investigation. Limited proteolysis experiments, for example, have demonstrated that the MMTS-inactivated enzyme is much more sensitive to trypsin digestion (data not shown).

DISCUSSION

BaCoADR-RHD Summary. The structural characterization and catalytic properties presented for *Ba*CoADR-RHD in this report represent the first crystallographic analysis for any member of the multidomain proteins class of the rhodanese superfamily (*24*). Given the well-characterized CoADR enzymes from *S. aureus* and *B. anthracis*, this work also describes a new isoform within group 3 of the flavoprotein disulfide reductase family (*15*). As such, the contributions of these enzymes to the biologically important topics of sulfur (and persulfide) trafficking and sulfide metabolism in prokaryotes (*1*, *24*, *68*) can now be more clearly appreciated. The dimeric *Ba*CoADR-RHD structure demonstrates that the two active-site Cys residues, Cys44 of the CoADR module and Cys514′ of the RHD′ domain, are separated by 25 Å. In contrast to *Ba*CoADR, the adenine end of bound CoAS− interacts extensively with the RHD′ domain and is well-buried, anchoring it firmly in the protein. This likely contributes to the observation that *Ba*CoADR-RHD does not recognize CoAD as a substrate. Reductive titration of the wild-type enzyme with NADH demonstrates flavin-mediated reduction of Cys44-SSCoA; synchrotron reduction gives a two-electron reduced (Cys44-SH + CoASH) enzyme as well, and the adenosine 3′-phosphate 5′-pyrophosphate of bound CoASH remains well-ordered in this structure. The pantetheine arm, however, becomes mobile; these observations lead to a swinging pantetheine arm model by which bound CoASH shuttles reducing equivalents from the CoADR active site to the RHD′ domain, bridging the 25 Å gap.

MMTS and DTNB are alternate disulfide substrates for *Ba*CoADR-RHD, but in mechanisms that are very distinct. MMTS reacts, as in the case of *Sa*CoADR, at the CoADR active site; the C44S mutant is inactive, but the C514S mutant retains activity. DTNB, which is not a substrate for *Sa*CoADR (*67*), reacts at Cys514′ but requires communication (the swinging pantetheine arm) between Cys44 and Cys514′; both C44S and C514S mutants have little or no activity. The swinging pantetheine arm and both Cys44 and Cys514′ are essential to the inactivation of *Ba*CoADR-RHD observed in turnover with MMTS, as analyzed by ESI-TOF mass spectrometry.

CoADR-RHD and S^0/S_n^{2-} *Reduction*. The CoADR-RHD isoform is found in *Sh. loihica*, in *B. anthracis* and several other bacterial pathogens, and in the antitumor agent

C. novyi-NT. A distinct CoADR-RHD-SirA-DsrE isoform has been identified in the Fe(III)-reducing anaerobe *P. carbinolicus* (*49*) and in several clostridia, including *C. botulinum* (*51*) and *Clostridium beijerinckii* (GenBank entry CP000721), another known Fe(III) reducer (*69*). In the latter isoform, the ~70-residue SirA module appears to be another sulfur-transfer protein as it is 43% identical in sequence to the *E. coli* TusA protein (*7*, *8*) (see the introductory section) and conserves the active-site CP*x*P motif involved directly in Cys-SSH-based sulfur relay. The DsrE domain of ca. 150 residues conserves the active-site Cys of *E. coli* TusD (*9*) (Cys78, which is equivalent to Cys781 of the *P. carbinolicus* multidomain enzyme) that accepts sulfur from the TusA persulfide; this Cys is also conserved in the *A. vinosum* DsrE protein (*11*) (see the introductory section), which is a structural homologue of TusD. These observations support a proposed role in sulfur transfer for the DsrE domain as well, in this third CoADR isoform; the Pcar_0429 gene encoding *P. carbinolicus* CoADR-RHD-SirA-DsrE was upregulated >20-fold during sulfur-dependent growth on Fe(III), compared with fermentative growth on acetoin (*49*). This is consistent with a possible function in reducing S^0 to HS^-, with HS^- serving as the intermediate in Fe(III) reduction at the cell surface.

The Pcar_1579 gene encoding CoADR-RHD was upregulated 5-fold during sulfur-dependent growth of *P. carbinolicus* on Fe(III) (*49*), and Lukose et al. (*17*) demonstrated that the *Sh. loihica* enzyme catalyzed the NADH-dependent reduction of polysulfide: $NADH + S_4^{2-} \rightarrow S_3^{2-} + HS^- + NAD^+$ [see the introductory section (Scheme 2)]. Sequence comparisons have shown that the polysulfide-sulfur transferase (Sud) protein from *W. succinogenes* contains a catalytic loop very similar to that of the RhdA rhodanese and the RHDs; an NMR structure is available for the sulfur-loaded form of the Sud protein and includes a calculated model for the Cys89-SS_5H polysulfide tail (*54*). The positively charged binding pocket consists of Arg46, Lys90, and Arg94 of the catalytic loop and one other active-site Arg residue; Arg46 and Arg94 are conserved in all RHDs, and Lys90 is either conserved or replaced with Arg in the *P. carbinolicus* and clostridial enzymes (Figure 3B) (aligned with *Ba*CoADR-RHD residues 476, 515, and 519). The fourth active-site Arg of the Sud protein appears in the segment equivalent to RhdA residues 200−209 that is absent in the RHD domains. All things considered, we conclude that the Cys514 equivalent in *Sh. loihica* CoADR-RHD (Cys531) is the primary S_{4-5}^{2-} reaction site. While the Sud protein transfers its polysulfide ligand to the active site of polysulfide reductase (*18*, *54*), *Sh. loihica* CoADR-RHD both binds and reduces polysulfide to HS^-, as demonstrated by Lukose et al. (*17*).

Scheme 2A (see the introductory section) represents one of two mechanistic proposals forwarded to account for polysulfide binding and reduction by the *Sh. loihica* enzyme. Our structural and kinetic analysis of *Ba*CoADR-RHD (50% identical in sequence) leads to the following points. (1) There is no provision for restoring the Cys-SSCoA disulfide in the resting, oxidized enzyme. (2) The distance between Cys43-S_γ and Cys531′-S_γ is ca. 25 Å. In the model of the Sud protein Cys89-SS_5H polysulfide tail, the distance between S1 and S5 is 5.3 Å (*54*). These considerations make it extremely unlikely that there could be direct chemical interaction between Cys43-S_γ and Cys531′-SS_4H. (3) On the basis of the characterization of the DTNB reaction with *Ba*CoADR-RHD, as presented in Scheme 5, both the initial reaction with S_4^{2-} at Cys531′ and the requirement for communication with the active site of the CoADR module are supported, but the direct reaction of Cys43 with Cys531′-SS_4H is extremely unlikely.

Scheme 7: Proposed Mechanism for Polysulfide Reduction by CoADR-RHD[a]

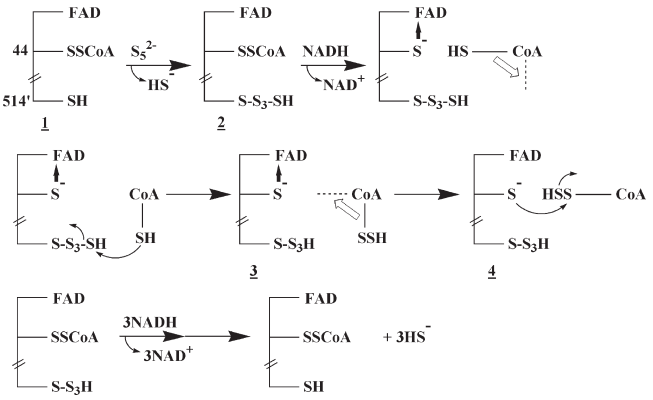

[a]Numbered intermediates correspond to enzyme states given in Scheme 5.

As described in Scheme 7, our mechanistic proposal for polysulfide reduction by CoADR-RHD begins with an enzyme form in which (1) S_5^{2-} has reacted at Cys514′ (*Ba*CoADR-RHD numbering) and (2) NADH has reduced the Cys44-SSCoA disulfide. The swinging pantetheine arm of tightly bound, reduced CoASH moves into position close to the polysulfide; attack by the pantetheine-S^- on the terminal sulfur of Cys514′-SS_4H yields the nascent pantetheine-SSH persulfide, reducing the polysulfide tail by one *S* unit. This structure is analogous to species 3 in Scheme 5. The swinging arm now moves back to its original position, delivering the persulfide for thiol interchange with Cys44-S^-. The Cys44-SSCoA disulfide re-forms, restoring the resting, oxidized enzyme (with Cys514′-SS_3H, analogous to species 2 in Scheme 5) and releasing HS^-. The cycle is repeated three times to complete the reduction of S_5^{2-} to $5HS^-$. The overall reaction can be contrasted with that described for sulfide:quinone oxidoreductase (*12*) [see the introductory section (Scheme 1)], which converts HS^- to polysulfide at the expense of a quinone oxidant; the mechanisms are mirror images, working in opposite directions. CoADR-RHD converts $5NADH + S_5^{2-} \rightarrow 5NAD^+ + 5HS^-$; sulfide:quinone oxidoreductase converts $5HS^- + 5Q \rightarrow S_5^{2-} + 5QH_2$. Cys514′ is the functional equivalent of sulfide:quinone oxidoreductase Cys350, and the swinging pantetheine arm is essential for connection with Cys44.

The polysulfide reduction catalyzed by *Sh. loihica* CoADR-RHD may be complemented by reactions with other sulfur donors such as thiosulfate and 3-mercaptopyruvate; the RHD active sites of *E. coli* ThiI and human MOCS3 (see the introductory section) accept sulfur directly from free cysteine, as catalyzed by IscS (*3*) and Nfs1 (*70*) desulfurases, respectively. Reduction of the Cys-SSCoA disulfide promotes the movement of the swinging pantetheine-SH arm and reaction of the latter with RHD Cys-SSH. The nascent pantetheine-SSH swings back into position near the Cys of the CoADR module, where HS^- is released or transferred. In the mechanisms proposed for *E. coli* ThiI (*3*) and human MOCS3 (*4*), formation or transfer of the HS^- equivalent involves an interdomain protein disulfide intermediate, which must be reduced in the catalytic cycle. In CoADR-RHD turnover, the same formation or transfer of the HS^- equivalent involves re-formation of the Cys-SSCoA disulfide; NADH serves as the catalytic reductant. For the *P.*

carbinolicus CoADR-RHD, the nascent HS^- equivalent has been suggested to serve as the intermediate in Fe(III) reduction at the cell surface (*49*). In the CoADR-RHD-SirA-DsrE isoform, the terminal sulfur could be transferred directly from the Cys529-SSH persulfide (*P. carbinolicus* numbering) to the active-site Cys591 of the SirA domain, in a cascade leading ultimately to the DsrE domain Cys781. *B. anthracis* Sterne, while lacking this third CoADR isoform, does have CoADR-RHD (BAS0736), SirA-RHD (BAS0738; YrkF homologue), SirA (BAS0740; TusA homologue), and DsrE-like (BAS0743; YrkE homologue) protein-encoding loci clustered together.[2] In *B. anthracis*, the ThiI protein is also known to lack the C-terminal RHD found in *E. coli* ThiI (*71*); *Ba*CoADR-RHD could function to provide the HS^- equivalent needed by ThiI for 4-thiouridine-tRNA synthesis.

A Possible Role for BaCoADR-RHD in the Sporulation—Germination Cycle. There are several indications for sporulation-specific functions involving sulfur metabolism and low-molecular weight thiols such as Cys and CoASH in *B. subtilis* and *B. anthracis*. The BAS0736 gene (Sterne strain) encoding *Ba*CoADR-RHD is expressed at low levels in late log phase (*23*) but is upregulated ca. 4-fold during sporulation.[5] The transcript is present at even higher levels (ca. 20—30-fold increase) during the first 60 min after inoculation, which corresponds to germination and outgrowth. The BASΔ0736 deletion mutant[6] grows normally in brain heart infusion broth but appears significantly compromised both in germination assays and in resuming exponential growth following exposure to the disulfide stress reagent diamide. Crow et al. (*72*) have recently reported the crystal structure and functional analysis of the *B. subtilis* thiol-disulfide oxidoreductase StoA, which is an extracytoplasmic enzyme important for synthesis of the spore core peptidoglycan. The bifunctional enzyme MiaB catalyzes linked thiolation and methylation reactions in the conversion of N6-isopentenyladenosine at position 37 of $tRNA^{Tyr}$ to N6-isopentenyl-2-thiomethyladenosine (*73*), and this methylthiolation modification has been suggested to relate to sporulation in *B. subtilis* (*74*). The putative MiaB gene product (NP_389583) has been identified in *B. subtilis* strain 168 (*75*). The *B. subtilis* spore photoproduct lyase is a [4Fe-4S] enzyme that relies on the essential Cys141, possibly involving a cysteinyl radical intermediate, in the repair of thymine dimers that result from UV irradiation of *B. subtilis* spores (*76*). This enzyme is a major factor in the extreme resistance of sporulating cells to UV radiation. Cysteine is the major low-molecular weight thiol in *B. subtilis* (*22*), and the *yubC* gene encoding cysteine dioxygenase ($Cys\text{-}SH + O_2 \rightarrow Cys\text{-}SO_2^-$) is significantly upregulated during sporulation (*77*). A *yubC* mutant was able to form spores, but with a reduced efficiency. These results suggest that further evaluation of CoADR-RHD, which is found in a number of spore-forming bacterial pathogens (e.g., *B. anthracis* and *C. botulinum*), should be pursued as a potential target for the design of therapeutic agents.

REFERENCES

1. Mueller, E. G. (2006) Trafficking in persulfides: Delivering sulfur in biosynthetic pathways. *Nat. Chem. Biol. 2*, 185–194.
2. Palenchar, P. M., Buck, C. J., Cheng, H., Larson, T. J., and Mueller, E. G. (2000) Evidence that ThiI, an enzyme shared between thiamin and 4-thiouridine biosynthesis, may be a sulfurtransferase that proceeds through a persulfide intermediate. *J. Biol. Chem. 275*, 8283–8286.
3. Mueller, E. G., Palenchar, P. M., and Buck, C. J. (2001) The role of the cysteine residues of ThiI in the generation of 4-thiouridine in tRNA. *J. Biol. Chem. 276*, 33588–33595.
4. Matthies, A., Rajagopalan, K. V., Mendel, R. R., and Leimkühler, S. (2004) Evidence for the physiological role of a rhodanese-like protein for the biosynthesis of the molybdenum cofactor in humans. *Proc. Natl. Acad. Sci. U.S.A. 101*, 5946–5951.
5. Matthies, A., Nimtz, M., and Leimkühler, S. (2005) Molybdenum cofactor biosynthesis in humans: Identification of a persulfide group in the rhodanese-like domain of MOCS3 by mass spectrometry. *Biochemistry 44*, 7912–7920.
6. Krepinsky, K., and Leimkühler, S. (2007) Site-directed mutagenesis of the active site loop of the rhodanese-like domain of the human molybdopterin synthase sulfurase MOCS3. Major differences in substrate specificity between eukaryotic and bacterial homologs. *FEBS J. 274*, 2778–2787.
7. Ikeuchi, Y., Shigi, N., Kato, J., Nishimura, A., and Suzuki, T. (2006) Mechanistic insights into sulfur relay by multiple sulfur mediators involved in thiouridine biosynthesis at tRNA wobble positions. *Mol. Cell 21*, 97–108.
8. Katoh, E., Hatta, T., Shindo, H., Ishii, Y., Yamada, H., Mizuno, T., and Yamazaki, T. (2000) High precision NMR structure of YhhP, a novel *Escherichia coli* protein implicated in cell division. *J. Mol. Biol. 304*, 219–229.
9. Numata, T., Fukai, S., Ikeuchi, Y., Suzuki, T., and Nureki, O. (2006) Structural basis for sulfur relay to RNA mediated by heterohexameric TusBCD complex. *Structure 14*, 357–366.
10. Numata, T., Ikeuchi, Y., Fukai, S., Suzuki, T., and Nureki, O. (2006) Snapshots of tRNA sulphuration via an adenylated intermediate. *Nature 442*, 419–424.
11. Dahl, C., Schulte, A., Stockdreher, Y., Hong, C., Grimm, F., Sander, J., Kim, R., Kim, S.-H., and Shin, D. H. (2008) Structural and molecular genetic insight into a widespread sulfur oxidation pathway. *J. Mol. Biol. 384*, 1287–1300.
12. Brito, J. A., Sousa, F. L., Stelter, M., Bandeiras, T. M., Vonrhein, C., Teixeira, M., Pereira, M. M., and Archer, M. (2009) Structural and functional insights into sulfide:quinone oxidoreductase. *Biochemistry 48*, 5613–5622.
13. Chen, Z. W., Koh, M., Van Driessche, G., Van Beeumen, J. J., Bartsch, R. G., Meyer, T. E., Cusanovich, M. A., and Mathews, F. S. (1994) The structure of flavocytochrome c sulfide dehydrogenase from a purple phototrophic bacterium. *Science 266*, 430–432.
14. Ojha, S., Meng, E. C., and Babbitt, P. C. (2007) Evolution of function in the "two dinucleotide binding domains" flavoproteins. *PLoS Comput. Biol. 3*, e121.
15. Argyrou, A., and Blanchard, J. S. (2004) Flavoprotein disulfide reductases: Advances in chemistry and function. *Prog. Nucleic Acid Res. Mol. Biol. 78*, 89–142.
16. Mallett, T. C., Wallen, J. R., Karplus, P. A., Sakai, H., Tsukihara, T., and Claiborne, A. (2006) Structure of coenzyme A-disulfide reductase from *Staphylococcus aureus* at 1.54 Å resolution. *Biochemistry 45*, 11278–11289.
17. Lukose, V., Lopez, K., and Crane, E. J., III (2008) Discovery and characterization of an NADH-dependent polysulfide reductase flavoprotein (Npsr) from *Shewanella loihica* PV-4: Implications for dissimilatory sulfur reduction in the genus *Shewanella*. In Flavins and Flavoproteins 2008 (Medina, M., Ed.) pp 375—380, Prensas Universitarias de Zaragoza, Zaragoza, Spain.
18. Hedderich, R., Klimmek, O., Kröger, A., Dirmeier, R., Keller, M., and Stetter, K. O. (1999) Anaerobic respiration with elemental sulfur and with disulfides. *FEMS Microbiol. Rev. 22*, 353–381.
19. Luba, J., Charrier, V., and Claiborne, A. (1999) Coenzyme A-disulfide reductase from *Staphylococcus aureus*: Evidence for asymmetric behavior on interaction with pyridine nucleotides. *Biochemistry 38*, 2725–2737.
20. Wallen, J. R., Paige, C., Mallett, T. C., Karplus, P. A., and Claiborne, A. (2008) Pyridine nucleotide complexes with *Bacillus anthracis* coenzyme A-disulfide reductase: A structural analysis of dual NAD(P)H specificity. *Biochemistry 47*, 5182–5193.
21. Nicely, N. I., Parsonage, D., Paige, C., Newton, G. L., Fahey, R. C., Leonardi, R., Jackowski, S., Mallett, T. C., and Claiborne, A. (2007) Structure of the type III pantothenate kinase from *Bacillus anthracis* at 2.0 Å resolution: Implications for coenzyme A-dependent redox biology. *Biochemistry 46*, 3234–3245.
22. Newton, G. L., Arnold, K., Price, M. S., Sherrill, C., delCardayre, S. B., Aharonowitz, Y., Cohen, G., Davies, J., Fahey, R. C., and

[2] A. Claiborne, unpublished observations.
[5] N. Bergman, personal communication.
[6] C. Paige, S. D. Reid, P. C. Hanna, and A. Claiborne, unpublished experiments.

Davis, C. (1996) Distribution of thiols in microorganisms: Mycothiol is a major thiol in most actinomycetes. *J. Bacteriol. 178*, 1990–1995.
23. Bergman, N. H., Anderson, E. C., Swenson, E. E., Niemeyer, M. M., Miyoshi, A. D., and Hanna, P. C. (2006) Transcriptional profiling of the *Bacillus anthracis* life cycle in vitro and an implied model for regulation of spore formation. *J. Bacteriol. 188*, 6092–6100.
24. Cipollone, R., Ascenzi, P., and Visca, P. (2007) Common themes and variations in the rhodanese superfamily. *IUBMB Life 59*, 51–59.
25. Nelson, K. J., Parsonage, D., Hall, A., Karplus, P. A., and Poole, L. B. (2008) Cysteine pK_a values for the bacterial peroxiredoxin AhpC. *Biochemistry 47*, 12860–12868.
26. Miller, H., and Claiborne, A. (1991) Peroxide modification of monoalkylated glutathione reductase. Stabilization of an active-site cysteine-sulfenic acid. *J. Biol. Chem. 266*, 19342–19350.
27. Riddles, P. W., Blakeley, R. L., and Zerner, B. (1979) Ellman's reagent: 5,5′-Dithiobis(2-nitrobenzoic acid)—a reexamination. *Anal. Biochem. 94*, 75–81.
28. Stura, E. A. (1999) Seeding. In Protein Crystallization: Techniques, Strategies, and Tips (Bergfors, T. M., Ed.) pp 139−154, International University Line, La Jolla, CA.
29. Otwinowski, Z., and Minor, W. (1997) Processing of X-ray diffraction data collected in oscillation mode. *Methods Enzymol. 276*, 307–326.
30. Pflugrath, J. W. (1999) The finer things in X-ray diffraction data collection. *Acta Crystallogr. D55*, 1718–1725.
31. Terwilliger, T. C., and Berendzen, J. (1999) Automated MAD and MIR structure solution. *Acta Crystallogr. D55*, 849–861.
32. Collaborative Computational Project Number 4 (1994) The CCP4 suite: Programs for protein crystallography. *Acta Crystallogr. D50*, 760–763.
33. Terwilliger, T. C. (2000) Maximum-likelihood density modification. *Acta Crystallogr. D56*, 965–972.
34. Terwilliger, T. C. (2003) Automated main-chain model building by template matching and iterative fragment extension. *Acta Crystallogr. D59*, 38–44.
35. Jones, T. A., Zou, J. Y., Cowan, S. W., and Kjeldgaard, M. (1991) Improved methods for building protein models in electron-density maps and the location of errors in these models. *Acta Crystallogr. A47*, 110–119.
36. Brunger, A. T., Adams, P. D., Clore, G. M., DeLano, W. L., Gros, P., Grosse-Kunstleve, R. W., Jiang, J. S., Kuszewski, J., Nilges, M., Pannu, N. S., Read, R. J., Rice, L. M., Simonson, T., and Warren, G. L. (1998) Crystallography & NMR system: A new software suite for macromolecular structure determination. *Acta Crystallogr. D54*, 905–921.
37. Winn, M. D., Isupov, M. N., and Murshudov, G. N. (2001) Use of TLS parameters to model anisotropic displacements in macromolecular refinement. *Acta Crystallogr. D57*, 122–133.
38. Murshudov, G. N., Vagin, A. A., and Dodson, E. J. (1997) Refinement of macromolecular structures by the maximum-likelihood method. *Acta Crystallogr. D53*, 240–255.
39. Emsley, P., and Cowtan, K. (2004) Coot: Model-building tools for molecular graphics. *Acta Crystallogr. D60*, 2126–2132.
40. Holm, L., and Sander, C. (1993) Protein structure comparison by alignment of distance matrices. *J. Mol. Biol. 233*, 123–138.
41. Holm, L., and Park, J. (2000) DaliLite workbench for protein structure comparison. *Bioinformatics 16*, 566–567.
42. Thompson, J. D., Higgins, D. G., and Gibson, T. J. (1994) CLUSTAL W: Improving the sensitivity of progressive multiple sequence alignment through sequence weighting, position-specific gap penalties and weight matrix choice. *Nucleic Acids Res. 22*, 4673–4680.
43. Morgenstern, B. (2004) DIALIGN: Multiple DNA and protein sequence alignment at BiBiServ. *Nucleic Acids Res. 32*, W33–W36.
44. Gouet, P., Courcelle, E., Stuart, D. I., and Metoz, F. (1999) ESPript: Analysis of multiple sequence alignments in PostScript. *Bioinformatics 15*, 305–308.
45. DeLano, W. L. (2002) The PyMOL Molecular Graphics System, DeLano Scientific, San Carlos, CA.
46. Jönsson, T. J., Tsang, A. W., Lowther, W. T., and Furdui, C. M. (2008) Identification of intact protein thiosulfinate intermediate in the reduction of cysteine sulfinic acid in peroxiredoxin by human sulfiredoxin. *J. Biol. Chem. 283*, 22890–22894.
47. Charrier, V., Luba, J., Parsonage, D., and Claiborne, A. (2000) Limited proteolysis as a structural probe of the soluble α-glycerophosphate oxidase from *Streptococcus* sp. *Biochemistry 39*, 5035–5044.
48. Krauth-Siegel, R. L., Arscott, L. D., Schönleben-Janas, A., Schirmer, R. H., and Williams, C. H. Jr. (1998) Role of active site tyrosine residues in catalysis by human glutathione reductase. *Biochemistry 37* 13968–13977.
49. Haveman, S. A., DiDonato, R. J. Jr., Villanueva, L., Shelobolina, E. S., Postier, B. L., Xu, B., Liu, A., and Lovley, D. R. (2008) Genome-wide gene expression patterns and growth requirements suggest that *Pelobacter carbinolicus* reduces Fe(III) indirectly via sulfide production. *Appl. Environ. Microbiol. 74*, 4277–4284.
50. Karplus, P. A., and Schulz, G. E. (1989) Substrate binding and catalysis by glutathione reductase as derived from refined enzyme: substrate crystal structures at 2 Å resolution. *J. Mol. Biol. 210*, 163–180.
51. Sebaihia, M., Peck, M. W., Minton, N. P., Thomson, N. R., Holden, M. T., Mitchell, W. J., Carter, A. T., Bentley, S. D., Mason, D. R., Crossman, L., Paul, C. J., Ivens, A., Wells-Bennik, M. H., Davis, I. J., Cerdeno-Tarraga, A. M., Churcher, C., Quail, M. A., Chillingworth, T., Feltwell, T., Fraser, A., Goodhead, I., Hance, Z., Jagels, K., Larke, N., Maddison, M., Moule, S., Mungall, K., Norbertczak, H., Rabbinowitsch, E., Sanders, M., Simmonds, M., White, B., Whithead, S., and Parkhill, J. (2007) Genome sequence of a proteolytic (Group I) *Clostridium botulinum* strain Hall A and comparative analysis of the clostridial genomes. *Genome Res. 17*, 1082–1092.
52. Bettegowda, C., Huang, X., Lin, J., Cheong, I., Kohli, M., Szabo, S. A., Zhang, X., Diaz, L. A. Jr., Velculescu, V. E., Parmigiani, G., Kinzler, K. W., Vogelstein, B., and Zhou, S. (2006) The genome and transcriptomes of the anti-tumor agent *Clostridium novyi-NT*. *Nat. Biotechnol. 24*, 1573–1580.
53. Bordo, D., Deriu, D., Colnaghi, R., Carpen, A., Pagani, S., and Bolognesi, M. (2000) The crystal structure of a sulfurtransferase from *Azotobacter vinelandii* highlights the evolutionary relationship between the rhodanese and phosphatase enzyme families. *J. Mol. Biol. 298*, 691–704.
54. Lin, Y.-J., Dancea, F., Löhr, F., Klimmek, O., Pfeiffer-Marek, S., Nilges, M., Wienk, H., Kröger, A., and Rüterjans, H. (2004) Solution structure of the 30 kDa polysulfide-sulfur transferase homodimer from *Wolinella succinogenes*. *Biochemistry 43*, 1418–1424.
55. Roberts, B. R., Wood, Z. A., Jönsson, T. J., Poole, L. B., and Karplus, P. A. (2005) Oxidized and synchrotron cleaved structures of the disulfide redox center in the N-terminal domain of *Salmonella typhimurium* AhpF. *Protein Sci. 14*, 2414–2420.
56. Berkholz, D. S., Faber, H. R., Savvides, S. N., and Karplus, P. A. (2008) Catalytic cycle of human glutathione reductase near 1 Å resolution. *J. Mol. Biol. 382*, 371–384.
57. Yun, M., Park, C. G., Kim, J. Y., Rock, C. O., Jackowski, S., and Park, H. W. (2000) Structural basis for the feedback regulation of *Escherichia coli* pantothenate kinase by coenzyme A. *J. Biol. Chem. 275*, 28093–28099.
58. Lai, J. R., Koglin, A., and Walsh, C. T. (2006) Carrier protein structure and recognition in polyketide and nonribosomal peptide biosynthesis. *Biochemistry 45*, 14869–14879.
59. Chirala, S. S., Jayakumar, A., Gu, Z.-W., and Wakil, S. J. (2001) Human fatty acid synthase: Role of interdomain in the formation of catalytically active synthase dimer. *Proc. Natl. Acad. Sci. U.S.A. 98*, 3104–3108.
60. Tang, Y., Kim, C.-Y., Mathews, I. I., Cane, D. E., and Khosla, C. (2006) The 2.7-Å crystal structure of a 194-kDa homodimeric fragment of the 6-deoxyerythronolide B synthase. *Proc. Natl. Acad. Sci. U.S.A. 103*, 11124–11129.
61. Donato, H., Krupenko, N. I., Tsybovsky, Y., and Krupenko, S. A. (2007) 10-Formyltetrahydrofolate dehydrogenase requires a 4′-phosphopantetheine prosthetic group for catalysis. *J. Biol. Chem. 282*, 34159–34166.
62. Crane, E. J., III, Parsonage, D., Poole, L. B., and Claiborne, A. (1995) Analysis of the kinetic mechanism of enterococcal NADH peroxidase reveals catalytic roles for NADH complexes with both oxidized and two-electron-reduced enzyme forms. *Biochemistry 34*, 14114–14124.
63. Kenyon, G. L., and Bruice, T. W. (1977) Novel sulfhydryl reagents. *Methods Enzymol. 47*, 407–430.
64. Davioud-Charvet, E., McLeish, M. J., Veine, D. M., Giegel, D., Arscott, L. D., Andricopulo, A. D., Becker, K., Muller, S., Schirmer, R. H., Williams, C. H. Jr. and Kenyon, G. L. (2003) Mechanism-based inactivation of thioredoxin reductase from *Plasmodium falciparum* by Mannich bases. Implication for cytotoxicity. *Biochemistry 42*, 13319–13330.
65. Serjeant, E. P., and Dempsey, B. (1979) Ionisation Constants of Organic Acids in Aqueous Solution, Pergamon Press, New York.
66. Bruice, T. W., and Kenyon, G. L. (1982) Novel alkyl alkanethiolsulfonate sulfhydryl reagents. Modification of derivatives of L-cysteine. *J. Protein Chem. 1*, 47–58.
67. delCardayre, S. B., Stock, K. P., Newton, G. L., Fahey, R. C., and Davies, J. E. (1998) Coenzyme A disulfide reductase, the primary low molecular weight disulfide reductase from *Staphylococcus aureus*.

Purification and characterization of the native enzyme. *J. Biol. Chem. 273*, 5744–5751.
68. Kessler, D. (2006) Enzymatic activation of sulfur for incorporation into biomolecules in prokaryotes. *FEMS Microbiol. Rev. 30*, 825–840.
69. Weber, K. A., Achenbach, L. A., and Coates, J. D. (2006) Microorganisms pumping iron: Anaerobic microbial iron oxidation and reduction. *Nat. Rev. Microbiol. 4*, 752–764.
70. Marelja, Z., Stöcklein, W., Nimtz, M., and Leimkühler, S. (2008) A novel role for human Nfs1 in the cytoplasm: Nfs1 acts as a sulfur donor for MOCS3, a protein involved in molybdenum cofactor biosynthesis. *J. Biol. Chem. 283*, 25178–25185.
71. Waterman, D. G., Ortiz-Lombardia, M., Fogg, M. J., Koonin, E. V., and Antson, A. A. (2006) Crystal structure of *Bacillus anthracis* ThiI, a tRNA-modifying enzyme containing the predicted RNA-binding THUMP domain. *J. Mol. Biol. 356*, 97–110.
72. Crow, A., Liu, Y., Möller, M. C., Le Brun, N. E., and Hederstedt, L. (2009) Structure and functional properties of *Bacillus subtilis* endospore-biogenesis factor StoA. *J. Biol. Chem. 284*, 10056–10066.
73. Hernandez, H., Pierrel, F., Elleingand, E., Garcia-Serres, R., Huynh, B. H., Johnson, M. K., Fontecave, M., and Atta, M. (2007) MiaB, a bifunctional radical-*S*-adenosylmethionine enzyme involved in the thiolation and methylation of tRNA, contains two essential [4Fe-4S] clusters. *Biochemistry 46*, 5140–5147.
74. Buu, A., Menichi, B., and Heyman, T. (1981) Thiomethylation of tyrosine transfer ribonucleic acid is associated with initiation of sporulation in *Bacillus subtilis*: Effect of phosphate concentration. *J. Bacteriol. 146*, 819–822.
75. Anton, B. P., Saleh, L., Benner, J. S., Raleigh, E. A., Kasif, S., and Roberts, R. J. (2008) RimO, a MiaB-like enzyme, methylthiolates the universally conserved Asp88 residue of ribosomal protein S12 in *Escherichia coli*. *Proc. Natl. Acad. Sci. U.S.A. 105*, 1826–1831.
76. Chandor-Proust, A., Berteau, O., Douki, T., Gasparutto, D., Ollagnier-de-Choudens, S., Fontecave, M., and Atta, M. (2008) DNA repair and free radicals, new insights into the mechanism of spore photoproduct lyase revealed by single amino acid substitution. *J. Biol. Chem. 283*, 36361–36368.
77. Dominy, J. E., Jr., Simmons, C. R., Karplus, P. A., Gehring, A. M., and Stipanuk, M. H. (2006) Identification and characterization of bacterial cysteine dioxygenases: A new route of cysteine degradation for Eubacteria. *J. Bacteriol. 188*, 5561–5569.